STIM1 is a core trigger of airway smooth muscle remodeling and hyperresponsiveness in asthma

Martin T. Johnson[a], Ping Xin[a,b,c], J. Cory Benson[a,b,c], Trayambak Pathak[a,b,c], Vonn Walter[d], Scott M. Emrich[a], Ryan E. Yoast[a], Xuexin Zhang[a], Gaoyuan Cao[e], Reynold A. Panettieri Jr.[e], and Mohamed Trebak[a,b,c,1]

[a]Department of Cellular and Molecular Physiology, The Pennsylvania State University College of Medicine, Hershey, PA 17033; [b]Department of Pharmacology and Chemical Biology, University of Pittsburgh School of Medicine, Pittsburgh, PA 15231; [c]Vascular Medicine Institute, University of Pittsburgh School of Medicine, Pittsburgh, PA 15231; [d]Department of Public Health Sciences, The Pennsylvania State University College of Medicine, Hershey, PA 17033; and [e]Rutgers Institute for Translational Medicine and Science, New Brunswick, NJ 08901

Edited by Mark Nelson, Department of Pharmacology, University of Vermont, Burlington, VT; received August 9, 2021; accepted November 19, 2021

Airway remodeling and airway hyperresponsiveness are central drivers of asthma severity. Airway remodeling is a structural change involving the dedifferentiation of airway smooth muscle (ASM) cells from a quiescent to a proliferative and secretory phenotype. Here, we show up-regulation of the endoplasmic reticulum Ca^{2+} sensor stromal-interacting molecule 1 (STIM1) in ASM of asthmatic mice. STIM1 is required for metabolic and transcriptional reprogramming that supports airway remodeling, including ASM proliferation, migration, secretion of cytokines and extracellular matrix, enhanced mitochondrial mass, and increased oxidative phosphorylation and glycolytic flux. Mechanistically, STIM1-mediated Ca^{2+} influx is critical for the activation of nuclear factor of activated T cells 4 and subsequent interleukin-6 secretion and transcription of pro-remodeling transcription factors, growth factors, surface receptors, and asthma-associated proteins. STIM1 drives airway hyperresponsiveness in asthmatic mice through enhanced frequency and amplitude of ASM cytosolic Ca^{2+} oscillations. Our data advocates for ASM STIM1 as a target for asthma therapy.

calcium signaling | asthma | smooth muscle remodeling | CRAC channels | metabolic reprogramming

Asthma is characterized as a chronic pulmonary disease with episodic or persistent airflow obstruction and affects ~339 million people globally (1). In addition, it is estimated to cost the United States ~81.9 billion dollars a year due to health care costs and productivity losses (2). Although many asthmatic patients have their symptoms under control with bronchodilators and corticosteroids, a significant subpopulation of these patients are refractory to these conventional treatments (3). Moreover, asthmatic patients have an accelerated decline in pulmonary function (4). Considering these high costs and morbidities, it is apparent that the current treatment modalities are inadequate, and additional studies are required to further understand the molecular mechanisms of asthma that could be targeted by novel therapies.

Although classically considered an inflammatory disease, increasing evidence points to the structural changes in the airways as key determinants in the pathogenesis of asthma (5). These structural changes, termed airway remodeling (AR), occur in both mild and severe asthmatics and tend to worsen with asthma severity (6, 7). AR includes goblet cell hyperplasia and metaplasia, fibrosis, thickening of the lamina reticularis, angiogenesis, and hyperplasia and hypertrophy of airway smooth muscle (ASM) (8). Specifically, ASM cells have been recognized as the effector cells of AR (5, 9, 10). During AR, ASM cells undergo a phenotypic switch from a quiescent and contractile phenotype into a synthetic phenotype. Synthetic ASM cells are highly proliferative, migratory, and secrete a plethora of cytokines and extracellular matrix molecules that worsen asthma outcome (11, 12).

Calcium (Ca^{2+}) signaling is a key regulator of numerous short-term and long-term cellular functions including contraction and activation of transcriptional programs that control proliferation, migration, secretion, and metabolism (13). Smooth muscle phenotypic switch is characterized by extensive remodeling of the cellular ion channel repertoire with major changes in expression and regulation of Ca^{2+} channels and transporters (14–21).The store-operated Ca^{2+} entry (SOCE) pathway has emerged as particularly critical for vascular smooth muscle and cardiomyocyte remodeling during cardiovascular disease (22, 23). SOCE is activated by the binding of agonists, growth factors, and inflammatory mediators to receptors coupled to phospholipase-C (PLC) isoforms. PLC induces the cleavage of phosphatidylinositol 4,5-bisphosphate into the soluble inositol-1,4,5-trisphosphate (IP_3) and the membrane-bound diacylglycerol. IP_3 is then able to diffuse to the endoplasmic reticulum (ER) and stimulate IP_3 receptors to deplete ER Ca^{2+} stores. ER Ca^{2+} store depletion causes Ca^{2+} to dissociate from the luminal EF-hand domains of the ER transmembrane protein, STIM1. This causes STIM1 to gain an extended conformation, oligomerize, and move into ER–plasma membrane junctions. At these junctions, STIM1 physically traps and activates the Ca^{2+} release–activated Ca^{2+} (CRAC) channels that are formed by hexamers of Orai proteins, leading to Ca^{2+} influx from the extracellular milieu into the cytosol (24, 25). Although mammals express another homolog of STIM1 called

Significance

Stromal-interacting molecule 1 (STIM1) proteins are essential for the function of store-operated Ca^{2+} entry (SOCE). Using transcriptomics, metabolomics, imaging, and inducible smooth muscle–specific STIM1 knockout mice expressing genetically encoded Ca^{2+} sensors, we reveal a crucial function of STIM1 in airway remodeling and airway hyperresponsiveness in asthma. STIM1-mediated Ca^{2+} oscillations in airway smooth muscle (ASM) cells are critical for ASM remodeling through metabolic and transcriptional reprogramming and cytokine secretion, including IL-6. These effects are driven by Ca^{2+}-dependent activation of the transcription factor isoform NFAT4 specifically in ASM. Our data provide evidence that ASM STIM1 and SOCE are central triggers of asthma manifestations and advocate for the future use of STIM1 as a molecular target in asthma therapy.

Author contributions: M.T.J. and M.T. designed research; M.T.J., P.X., J.C.B., T.P., and X.Z. performed research; S.M.E. and R.E.Y. contributed new reagents/analytic tools; M.T.J., V.W., and M.T. analyzed data; M.T.J. and M.T. wrote the paper; and G.C. and R.A.P. provided cells from healthy and asthmatic donors.

The authors declare no competing interest.

This article is a PNAS Direct Submission.

[1]To whom correspondence may be addressed. Email: trebakm@pitt.edu.

This article contains supporting information online at http://www.pnas.org/lookup/suppl/doi:10.1073/pnas.2114557118/-/DCSupplemental.

Published December 23, 2021.

STIM2, quiescent smooth muscle cells primarily express STIM1 (24, 26, 27). When activated by physiological concentrations of agonists, SOCE-mediated Ca^{2+} signals take the form of regenerative Ca^{2+} oscillations (28, 29), which are crucial for the activation of isoforms of Ca^{2+}-dependent transcription factors, including nuclear factor of activated T cells (NFAT) that drive transcriptional programs supporting proliferation, migration, metabolism, and cytokine secretion (30, 31).

By comparison to vascular smooth muscle and cardiomyocytes, very little is known about STIM1 and SOCE in ASM cells. Previous studies have shown that STIM1 is necessary for SOCE in cultured ASM cells (32, 33) and for ASM cell proliferation and migration induced by the chemoattractant, platelet-derived growth factor (PDGF)-BB (33, 34). Here, we hypothesize that STIM1 is a critical driver of ASM remodeling and airway hyperresponsiveness (AHR). We show that mice chronically challenged with the allergen house dust mite (HDM) have increased STIM1 protein expression in ASM. Using inducible smooth muscle–specific STIM1 knockout mice ($STIM1^{smKO}$), we reveal that STIM1 is a core trigger of AR and AHR in asthmatic mice. ASM STIM1 is required for agonist-induced Ca^{2+} oscillations, activation of the NFAT4 isoform, interleukin-6 (IL-6) secretion, enhanced metabolic activity, and the reprogramming of ASM into a pro-remodeling transcriptional program. Intriguingly, transcriptional profiling showed that the enhanced metabolic activity of synthetic ASM is controlled by STIM1 and mediated by changes in both mitochondrial and glycolytic functions. We propose that because ASM STIM1 is required for both AR and AHR in asthma, STIM1 is a potential molecular target in asthma therapy.

Results

Chronic Asthmatic Mice Show Increased STIM1 Expression in ASM. We generated $STIM1^{smKO}$ mice by crossing the current gold-standard tamoxifen-inducible smooth muscle Cre (Myh11 Cre) (35) with mice expressing *STIM1* loxP-flanked alleles ($STIM1^{fl/fl}$) (36). Two littermate controls were used for this study to control for both 1) an active Cre recombinase and 2) the presence of loxP sites: 1) Myh11 Cre mice intraperitonially injected with tamoxifen and 2) Myh11Cre $STIM1^{fl/fl}$ mice intraperitonially injected with vehicle. They will be henceforth referred to as 1) $Myh11^{Cre}$ and 2) $STIM1^{fl/fl}$. Genotyping of the tracheas from $STIM1^{smKO}$, $Myh11^{Cre}$, and $STIM1^{fl/fl}$ confirms that all cohorts have the transgenic $Myh11^{Cre}$, while the $STIM1^{smKO}$ and $STIM1^{fl/fl}$ mice have loxP-flanked alleles, and only the $STIM1^{smKO}$ mice have active Cre-Lox recombination. A $STIM1^{fl/fl}$ band can be seen in the STIM1 A reaction in the $STIM1^{smKO}$ cohort. It is likely that contaminating nonsmooth muscle tissue in these genotyping reactions from tracheas generate $STIM1^{fl/fl}$ PCR products in this cohort (*SI Appendix*, Fig. 1 *A* and *B*). Furthermore, Western blots of epithelium-denuded tracheas show that STIM1 protein expression is significantly reduced in the $STIM1^{smKO}$ mice compared to both the $Myh11^{Cre}$ and $STIM1^{fl/fl}$ littermates (Fig. 1 *A* and *B*). Interestingly, STIM2, another STIM homolog, was not detected in epithelium-denuded trachea from $Myh11^{Cre}$ mice. Splenic tissue, known for its high expression of STIM1 and STIM2 (36), was used as a positive control (*SI Appendix*, Fig. 1*C*).

We used a clinically relevant asthmatic model that intranasally sensitizes and challenges mice to the allergen HDM. Chronic exposures of HDM have been shown to induce AHR, airway inflammation, and AR and fibrosis in mice (37–39). $Myh11^{Cre}$ and $STIM1^{smKO}$ mice were both challenged with HDM according to the protocol described in Fig. 1*C*. As a control, two additional groups from both mice genotypes were challenged with saline. At the end of this HDM-challenge protocol (at day 49; Fig. 1*C*), lung slices were isolated and colabeled with the following antibodies: anti-smooth muscle α-actin conjugated to Cy3 (α-SMA; green) and anti-STIM1 with a secondary antibody conjugated to Alexa Fluor 647 (red). STIM1 fluorescence (red) was then quantified specifically in ASM (green) from all mice cohorts. HDM-challenged $Myh11^{Cre}$ mice showed significantly more STIM1 protein expression in ASM compared to the saline-challenged $Myh11^{Cre}$ mice. Importantly, both cohorts of the $STIM1^{smKO}$ mice had significantly reduced STIM1 expression specifically in ASM with prominent STIM1 staining in adjacent airway epithelial cells and surrounding lung tissue (Fig. 1 *D* and *E*). The isotype controls had no fluorescent labeling for STIM1 (*SI Appendix*, Fig. 1*D*).

STIM1 Is Required for AR in Chronic Asthmatic Mice. We and others have shown that STIM1 is necessary for remodeling of vascular smooth muscle during disease states, including chronic hypertension and restenosis (27, 40–43). Since AR shares morphological and mechanistic features with vascular remodeling (22), we reasoned that STIM1 might be necessary for AR in the chronic asthmatic HDM-challenge model. By labeling ASM in fixed lung slices with α-SMA and using immunohistochemistry (IHC), we observed that HDM-challenged $Myh11^{Cre}$ mice have increased ASM area as labeled with α-SMA (brown) compared to saline-challenged $Myh11^{Cre}$ mice, suggesting enhanced AR in agreement with previous findings (37–39). Remarkably, HDM-challenged $STIM1^{smKO}$ mice had significantly less ASM area compared to the HDM-challenged $Myh11^{Cre}$ mice. The saline-challenged $STIM1^{smKO}$ mice had similar ASM area to the saline-challenged $Myh11^{Cre}$ mice (Fig. 1 *F* and *G*). The isotype control antibody showed no IHC staining for α-SMA (*SI Appendix*, Fig. 1*E*). We also investigated fibrosis of these lung slices by using Masson's Trichrome staining, which labels collagen and extracellular matrix fibers in blue. Consistently, HDM-challenged $Myh11^{Cre}$ mice had significantly more Trichrome blue–stained area than the saline-challenged $Myh11^{Cre}$ mice, and the HDM-challenged $STIM1^{smKO}$ mice had dramatically less Trichrome blue staining than the HDM-challenged $Myh11^{Cre}$ mice. Furthermore, the saline-challenged $STIM1^{smKO}$ mice had similar levels of Trichrome blue staining as the saline-challenged $Myh11^{Cre}$ mice (Fig. 1 *H* and *I*).

A prominent feature of asthma is leukocyte recruitment into the airways. Indeed, HDM-challenged $Myh11^{Cre}$ mice had significantly more leukocytes in their bronchoalveolar lavage (BAL) than saline-challenged $Myh11^{Cre}$ mice (*SI Appendix*, Fig. 1*F*). These include monocytes, lymphocytes, neutrophils, and eosinophils (*SI Appendix*, Fig. 1*G*). Interestingly, saline-challenged and HDM-challenged $STIM1^{smKO}$ mice had similar proportions of BAL leukocyte populations as the saline-challenged and HDM-challenged $Myh11^{Cre}$ mice, respectively (*SI Appendix*, Fig. 1 *F* and *G*). These results suggest that ASM STIM1 is critical for the development of AR in asthma, including smooth muscle thickening and fibrosis, and that this phenotype is independent of leukocyte recruitment to the airways.

STIM1 Is Crucial for ASM Proliferation and Migration. To understand the molecular mechanisms by which STIM1 drives AR, we performed in vitro molecular studies on primary human ASM cells (HASMCs) (44). We have several cultures of HASMCs isolated from nonasthmatic and fatal asthmatic donors (*SI Appendix*, Fig. 2*A*). Cultured HASMCs express both STIM1 and STIM2, and we observed no difference in STIM1 and STIM2 protein expression between nonasthmatic and asthmatic donors using Western blotting (*SI Appendix*, Fig. 2 *B–D*). Furthermore, we measured SOCE among these donors using the ratiometric Ca^{2+} dye Fura2. HASMCs were stimulated first with 2 μM of the irreversible sarcoplasmic/endoplasmic reticulum Ca^{2+} ATPase (SERCA) inhibitor thapsigargin in a nominally Ca^{2+}-free bath solution to evaluate the extent of Ca^{2+} release from ER Ca^{2+} stores. Where indicated (*SI Appendix*, Fig. 2*E*), 2 mM Ca^{2+} was restored to the bath solution to

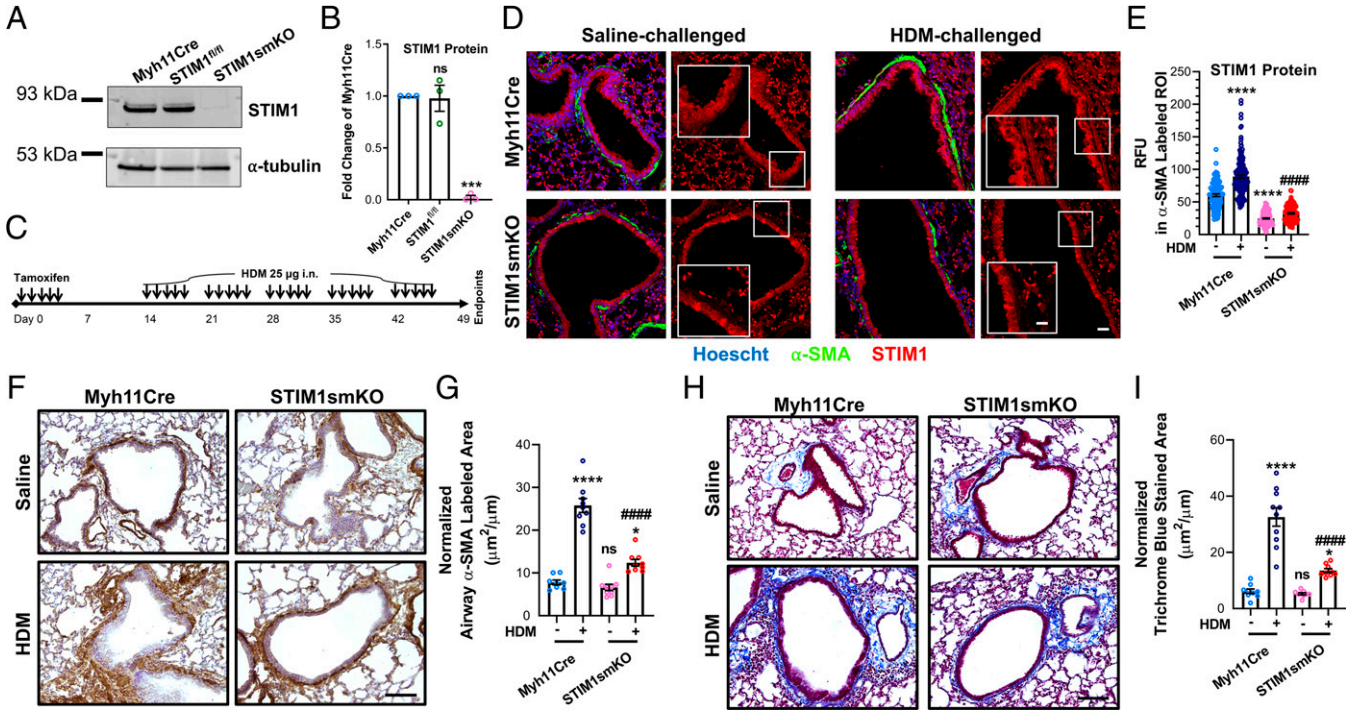

Fig. 1. ASM STIM1 protein is augmented in asthmatic mice and is necessary for AR. (*A*) Representative Western blot showing STIM1 protein in the epithelial-denuded tracheas from Myh11^{Cre}, STIM1$^{fl/fl}$, and STIM1^{smKO} mice. (*B*) Quantification of STIM1 protein from *A* in Myh11^{Cre} (n = 3), STIM1$^{fl/fl}$ (n = 3), and STIM1^{smKO} mice (n = 3) denuded tracheas using densitometry normalized to α-tubulin. (*C*) Scheme illustrating the time line of tamoxifen injections and intranasal HDM challenges. (*D*) Representative confocal images of lung slices from Myh11^{Cre} and STIM1^{smKO} mice challenged with either saline or HDM. Smooth muscle is labeled green with Cy3-congugated smooth muscle α-actin (α-SMA) antibody, STIM1 is labeled red with Alexa Flour 647 secondary and STIM1 antibody, and nuclei are counterstained blue with Hoescht. Images on the left are merged with all three colors, and images on the right only show STIM1. Zoomed insets focus on ASM. (Scale bars: 25 μm and 12.5 μm for inset.) (*E*) Quantification of relative fluorescence units (RFU; from many images like *D*) of STIM1 in regions of interest (ROIs) overlapping with α-SMA labeling in saline-challenged Myh11^{Cre} (n = 98), HDM-challenged Myh11^{Cre} (n = 185), saline-challenged STIM1^{smKO} (n = 143), and HDM-challenged STIM1^{smKO} mice (n = 122). (*F*) Representative immunohistochemistry images of lung slices from Myh11^{Cre} and STIM1^{smKO} mice challenged with either saline or HDM. Smooth muscle is labeled brown with α-SMA antibody and 3,3′-diaminobenzidine, and slides are counterstained with hematoxylin. (Scale bar: 100 μm.) (*G*) Quantification of α-SMA labeled area from *A* in saline-challenged Myh11^{Cre} (n = 8), HDM-challenged Myh11^{Cre} (n = 9), saline-challenged STIM1^{smKO} (n = 9), and HDM-challenged STIM1^{smKO} (n = 9) mice. (*H*) Representative images of lung slices stained with Masson's trichrome where collagen is stained blue. (Scale bar: 100 μm.) (*I*) Quantification of blue stained area from *C* in saline-challenged Myh11^{Cre} (n = 9), HDM-challenged Myh11^{Cre} (n = 10), saline-challenged STIM1^{smKO} (n = 9), and HDM-challenged STIM1^{smKO} (n = 9) mice. ns, not significant, *P < 0.05, ***P < 0.001, ****P < 0.0001 when compared to saline-challenged Myh11^{Cre}, ####P < 0.0001 when compared to HDM-challenged Myh11^{Cre} (one-way ANOVA with Dunnett's test for multiple comparisons).

measure the magnitude of SOCE. We found no difference in SOCE of HASMCs between nonasthmatic and asthmatic donors (*SI Appendix*, Fig. 2 *E–G*). Smooth muscle cells cultured in vitro dedifferentiate into a "synthetic" phenotype, remodel their Ca^{2+} signaling machinery, and up-regulate STIM proteins (11, 45, 46). Nevertheless, this in vitro dedifferentiation occurs equally in both nonasthmatic and asthmatic HASMCs, thus cancelling any in vivo differences between these two groups. This is consistent with results with vascular smooth muscle cells isolated from normotensive and hypertensive rats (41). Hence, for the remainder of our experiments, we used HASMCs from normal donors.

We generated stable STIM1 knockdown (KD) in HASMCs using two different small hairpin RNAs (shRNAs), and HASMCs stably expressing scrambled shRNA (shScramble) were used as a control. STIM1 protein expression was significantly diminished in shSTIM1#1 and shSTIM1#5 KD HASMCs compared to shScramble HASMCs (Fig. 2 *A* and *B*). Furthermore, SOCE was nearly eliminated in both STIM1 KD HASMCs conditions compared to shScramble control (Fig. 2 *D* and *E*). There was no compensation in either STIM2 (Fig. 2 *A* and *C*), or Orai1protein expression (*SI Appendix*, Fig. 3 *A–C*); both Orai1-α and Orai1-β translational variants were analyzed after protein sample deglycosylation as described in Methods. Using RT-qPCR, Orai2 and Orai3 messenger RNA (mRNA) expression was also comparable between shScramble and shSTIM1 conditions (*SI Appendix*, Fig. 3 *D* and *E*). We then assessed the role of STIM1 in HASMC migration and proliferation. HASMC migration was measured using the gap closure assay. To eliminate contributions from HASMC proliferation, media was supplemented with 10 μg/mL mitomycin C. Migration was significantly impaired in shSTIM1#1 and shSTIM1#5 KD HASMCs compared to shScramble HASMCs at 12 and 24 h (Fig. 2 *F* and *G*). Similarly, HASMC proliferation was measured over 72 h using the dye CyQUANT; shSTIM1#1 and shSTIM1#5 KD HASMCs had significant reduction in proliferation compared to shScramble HASMCs (Fig. 2*H*). We generated stable STIM1 KD HASMCs in another nonasthmatic donor (denoted as "donor 2"). STIM1 protein expression was also significantly reduced in shSTIM1#1 and shSTIM1#5 KD HASMCs compared to shScramble HASMCs from donor 2 (*SI Appendix*, Fig. 3 *F* and *G*). The proliferation and migration of HASMCs from donor 2 were also significantly decreased in shSTIM1#1 and shSTIM1#5 KD conditions compared to shScramble control (*SI Appendix*, Fig. 3 *H* and *I*). We costained shScramble, shSTIM1#1, and shSTIM1#5 HASMCs with 7-aminoactinomycin D (7-AAD) and Annexin V to determine the extent of apoptosis in these cell groups. There was no statistically significant change between the shSTIM1 and shScramble HASMCs in the percentage of cells in early (positive for Annexin V), late (double positive for Annexin V and 7AAD), or total

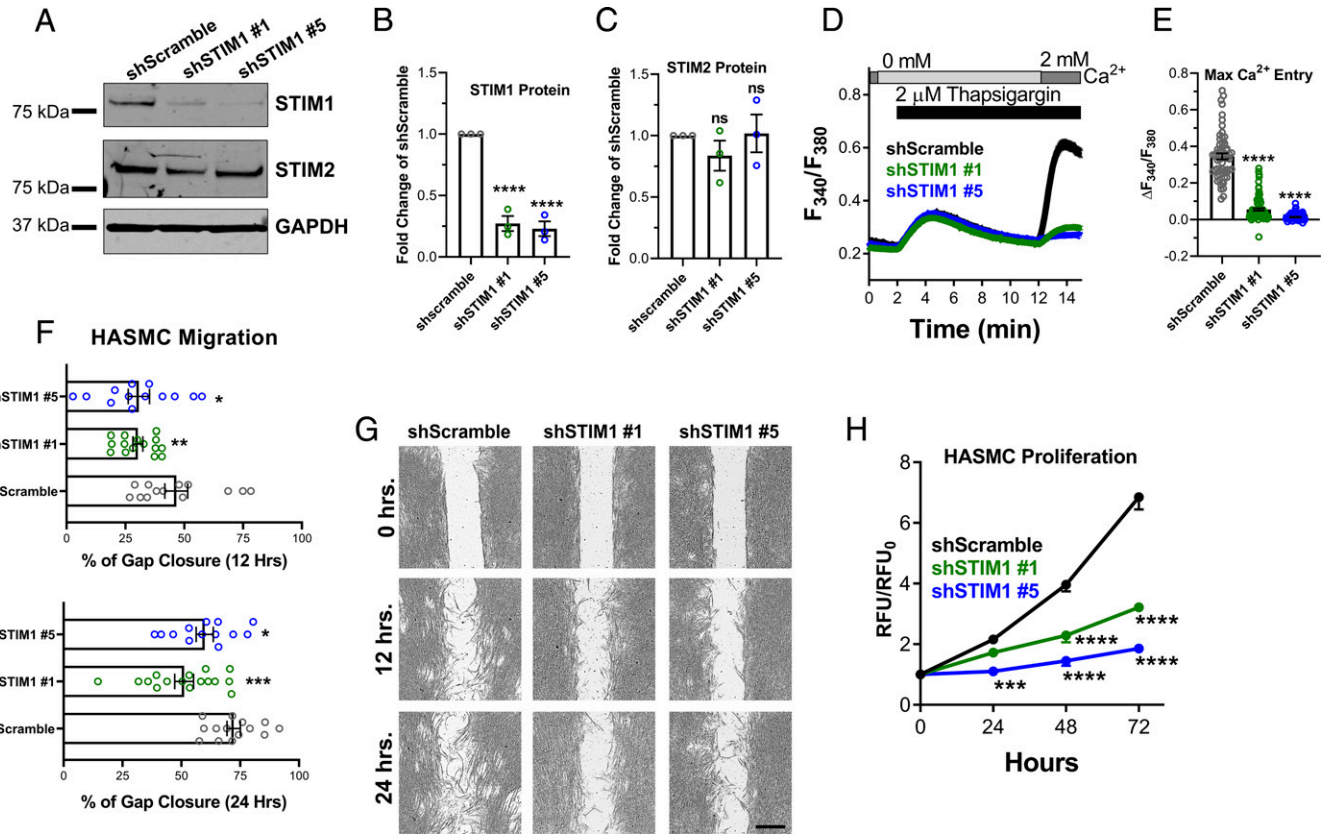

Fig. 2. STIM1 is necessary for ASM cell proliferation and migration. (*A*) Representative Western blots showing STIM1 and STIM2 protein expression in HASMCs transfected with either shScramble or with STIM1 shRNA (shSTIM1#1 or shSTIM1#5). (*B*) Quantification of STIM1 and (*C*) STIM2 protein expression in shScramble ($n = 3$), shSTIM1#1 ($n = 3$), and shSTIM1#5 ($n = 3$) HASMCs from *A* using densitometry normalized to GAPDH. (*D*) Cytosolic Ca^{2+} measurements using the standard Ca^{2+} off/Ca^{2+} on protocol with 2 μM thapsigargin showing SOCE activity in shScramble ($n = 61$; black trace), shSTIM1#1 ($n = 87$; green trace), and shSTIM1#5 ($n = 88$; blue trace) HASMCs. (*E*) Quantification of maximal SOCE from *D*. (*F*) Quantification of HASMC migration at 12 and 24 h in shScramble ($n = 13$), shSTIM1#1 ($n = 15$), and shSTIM1#5 ($n = 13$) HASMCs. (*G*) Representative bright-field images from *F*. (Scale bar: 500 μm.) (*H*) Quantification in normalized relative fluorescent units (RFU) of proliferation of shScramble ($n = 6$; black trace), shSTIM1#1 ($n = 6$; green trace), and shSTIM1#5 ($n = 6$; blue trace) HASMCs over 72 h. $^*P < 0.05$, $^{**}P < 0.01$, $^{***}P < 0.001$, $^{****}P < 0.0001$, ns = not significant (unpaired Student's *t* test for two comparisons and ANOVA with Dunnett's test for multiple comparisons).

apoptosis (sum of early and late apoptosis) (*SI Appendix*, Fig. 4 *A* and *B*). Furthermore, cleaved caspase 3 protein expression, which is a marker of apoptosis (47), was similar between shScramble, shSTIM1#1, and shSTIM1#5 HASMCs (*SI Appendix*, Fig. 4 *C–E*).

STIM1 Mediates Pro-remodeling Transcriptional Reprogramming in ASM. To identify downstream pathways regulated by STIM1 in ASM, we compared the transcriptional profiles of shScramble and shSTIM1 HASMCs using RNA sequencing (Dataset S3). Differential gene expression analysis revealed numerous genes significantly different between shScramble and shSTIM1#1 HASMCs (Fig. 3*A*) and between shScramble and shSTIM1#5 HASMCs (*SI Appendix*, Fig. 5*A*). Through gene set enrichment analysis (GSEA) using the reactome gene sets, numerous enriched pathways were revealed between shScramble and shSTIM1 HASMCs. Negatively enriched pathways found in shSTIM1 HASMCs include extracellular matrix organization, collagen formation, diseases of metabolism, metabolism of carbohydrates, signaling by PDGF, and mesenchymal to epithelial transition (MET) pathways that promote cell motility. Positively enriched pathways include DNA repair, interferon signaling, cholesterol biogenesis, and muscle contraction (Fig. 3 *B–F* and *SI Appendix*, Fig. 5 *B* and *C*). We validated several of these RNA-sequencing findings, especially targets involved in extracellular matrix production, using RT-qPCR. HASMCs transfected with shSTIM1#1 and shSTIM1#5 had significantly less COL5A2, LOX, and TGFβR1 mRNA than HASMCs transfected with shScramble (*SI Appendix*, Fig. 5 *D–F*). Expression profiling showed that STIM1 KD in HASMCs down-regulated the expression of pro-remodeling genes encoding transcription factors (MYC, FOXO1, KLF, ATF, FOS, and JUN), cytokines, agonists and receptors (IL-6, VEGF-A, TGFβ1/TGFβR1, Wnt2, Smoothened, and Patched1), signaling proteins (CaMK), and the orosomucoid-like 3 (ORMDL3) protein (48) that is specifically associated with human asthma (Fig. 3*G*). These transcriptional profiling results support a central function for STIM1 in promoting ASM dedifferentiation while suppressing the ASM quiescent phenotype.

STIM1 Is Required for NFAT4 Activation and Secretion of IL-6 by ASM Cells. We next sought to identify the mechanisms by which STIM1-mediated Ca^{2+} signals transcriptionally reprogram ASM to be "synthetic." SOCE has been well characterized in providing a specific spatiotemporal Ca^{2+} microdomain that stimulates the phosphatase calcineurin, which dephosphorylates numerous phosphorylation sites on the transcription factor NFAT, causing its translocation to the nucleus (28, 49, 50). Once in the nucleus, NFAT activates the transcription of other transcription factors, receptors, channels, and signaling pathways, including ones involved in proliferation, migration, and secretion (49). Furthermore, others have confirmed that NFAT4 (*NFATC3*) is the predominant NFAT isoform expressed

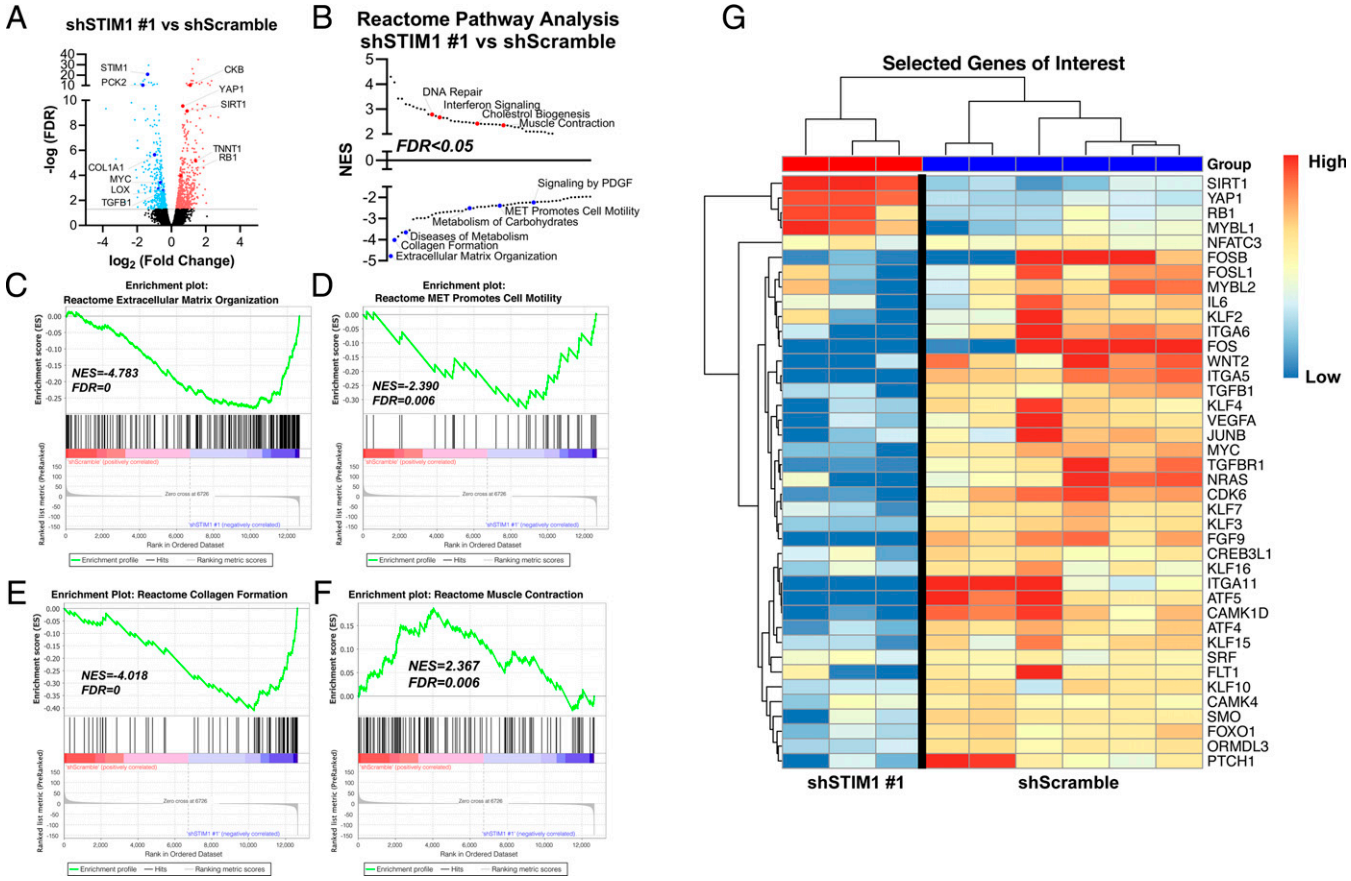

Fig. 3. STIM1 controls pro-remodeling transcriptional reprogramming. (*A*) Volcano plot comparing differentially expressed genes between shScramble and shSTIM1#1 HASMCs. Genes are plotted by $\log_2$ fold change and $-\log_{10}$ false discovery rate (FDR), with a threshold of an FDR <0.05 (gray line). In the shSTIM1#1 samples, significantly up-regulated and down-regulated genes are light red and light blue, respectively. (*B*) Pathway analysis using the reactome pathways gene set ranking significantly up-regulated (red) and down-regulated (blue) pathways based on normalized enrichment score (NES). (*C–F*) GSEA enrichment plots using the reactome pathways gene set comparing shSTIM1#1 and shScramble HASMCs showing a negative enrichment of extracellular matrix organization (*C*), MET promotes cell motility (*D*) and collagen formation genes (*E*), and a positive correlation in the enrichment of muscle contraction genes (*F*). For each GSEA enrichment plot, NES and FDR values are displayed. (*G*) Heatmap display of select genes, including major transcription factors, agonists, receptors, and effector proteins between HASMCs stably expressing shScramble and those expressing shSTIM1#1. Genes appear in rows, and samples appear in columns. Gene expression values were mean centered by gene.

in ASM cells (51–53). Following previously established techniques (54), we examined the ability of endogenous NFAT4 to be dephosphorylated in HASMCs upon maximal SOCE activation by 2 μM thapsigargin (*SI Appendix*, Fig. 5*G*). A total of 5 min after stimulation with thapsigargin, there was an increase in the proportion of dephosphorylated NFAT4 (NFAT4-deP) species relative to the phosphorylated species (NFAT4-P), as shown by shift in molecular weight on a Western blot. Importantly, both 1 μM cyclosporine (CsA), which inhibits calcineurin (55), and 5 μM gadolinium (Gd^{3+}), which specifically inhibits SOCE at these low concentrations (56), blocked NFAT4 dephosphorylation (*SI Appendix*, Fig. 5 *G* and *H*). Interestingly, even under unstimulated conditions, there was significantly less dephosphorylated NFAT4 in shSTIM1#1 and shSTIM1#5 HASMCs compared to shScramble HASMCs (Fig. 4 *A* and *B*). After stimulation with thapsigargin (at 5 min and 15 min), NFAT4 dephosphorylation in shSTIM1#1- and shSTIM1#5-transfected HASMCs was significantly inhibited compared to shScramble HASMCs (Fig. 4 *A* and *B*). We also stably expressed NFAT4m-Cherry in shSTIM1#1, shSTIM1#5, and shScramble HASMCs and followed its nuclear translocation using time-lapse fluorescence microscopy upon stimulation with 2 μM thapsigargin (Fig. 4 *C–F*). NFAT4mCherry translocated slower and significantly less in shSTIM1#1- and shSTIM1#5-transfected HASMCs as compared to shScramble HASMCs (Fig. 4 *C–F*). These results strongly indicate that NFAT4 activation and subsequent NFAT4-dependent signaling in ASM cells requires STIM1.

A significant property of ASM cells in asthma is their function as immune effectors that secrete inflammatory mediators, which further aggravate AR including smooth muscle proliferation, migration, and deposition of extracellular matrix (57–59). One such inflammatory mediator that requires SOCE and NFAT activation is IL-6 (60–63). Our RNA-sequencing findings showed that IL-6 expression in ASM cells is strongly down-regulated upon STIM1 KD (Fig. 3*G*). Thus, we sought to determine whether STIM1 is specifically required for the secretion of IL-6 in HASMCs. Using an enzyme-linked immunosorbent assay (ELISA), we measured IL-6 secretion in the media from serum-starved HASMCs stimulated with various asthma-related agonists (e.g., 500 nM Bradykinin [BK] and 100 μM methacholine [MeCh]), growth factors (20 ng/mL PDGF), and allergens (10 μg/mL HDM) in serum-free media for 18 h. All stimuli caused a significant increase in IL-6 secretion from HASMCs (Fig. 4*G* and *SI Appendix*, Fig. 5*I*). Interestingly, shSTIM1#1 and shSTIM1#5 KD HASMCs had significantly less IL-6 secretion than shScramble HASMCs in response to all stimuli. Furthermore, shScramble HASMCs treated with 1 μM CsA showed similar levels of stimulated IL-6 secretion to those of STIM1 KD HASMCs (Fig. 4*G* and *SI Appendix*, Fig. 5*I*), suggesting that IL-6 secretion requires calcineurin/NFAT

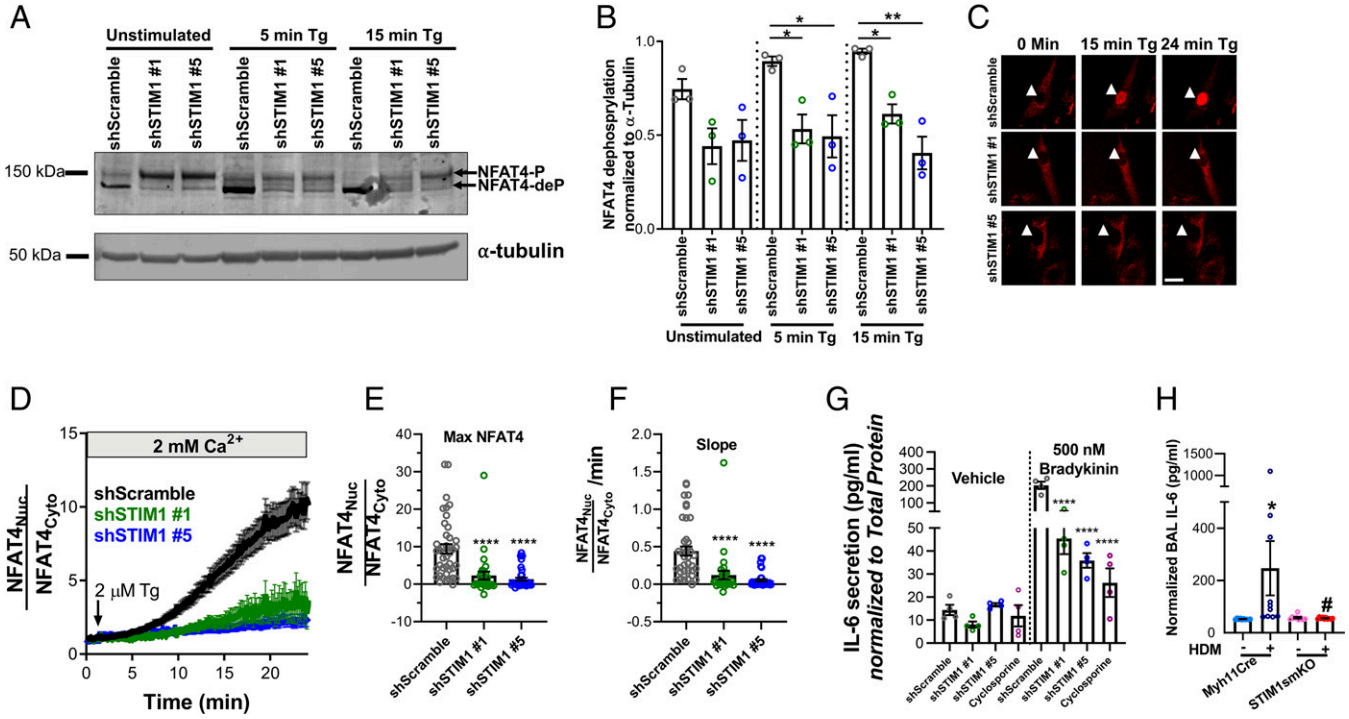

Fig. 4. STIM1 controls the activation of NFAT4. (*A*) Representative Western blot showing NFAT4-P and NFAT4-deP, respectively, in HASMCs transfected with shScramble, shSTIM1#1, or shSTIM1#5 and either unstimulated or stimulated for 5 or 15 min with 2 μM thapsigargin (Tg) in the presence of 2 mM Ca^{2+}. (*B*) Quantification of percentage of NFAT4-deP to NFAT-P in shScramble (n = 3), shSTIM1#1 (n = 3), and shSTIM1#5 (n = 3) HASMCs from *A* using densitometry normalized to α-tubulin. (*C*) Representative images of shScramble, shSTIM1#1, and shSTIM1#5 HASMCs expressing NFAT4mCherry that are either unstimulated (time 0) or stimulated with 2 μM Tg in the presence of 2 mM Ca^{2+} for 15 min and 24 min. White arrowheads point to the cell nucleus. (Scale bar: 25 μm.) (*D*) Time-lapsed quantification of nuclear NFAT4mcherry translocation of shScramble (n = 41; black trace), shSTIM1#1 (n = 29; green trace), and shSTIM1#5 (n = 35; blue trace) HASMCs stimulated with 2 μM Tg in the presence of 2 mM Ca^{2+}. Translocation is measured by dividing the fluorescence of a region of interest in the nucleus by that of a region of interest in the cytoplasm for each cell. Quantification of maximal (*E*) and slope (*F*) of NFAT4 translocation from *C*. (*G*) Using ELISA, IL-6 secretion is measured in shScramble (n = 4; gray circles), shSTIM1#1 (n = 4; green circles), shSTIM1#5 (n = 4; blue circles), and shScramble pretreated with 1 μM cyclosporine (n = 4; purple circles). HASMCs were stimulated overnight with either vehicle or 500 nM BK. For each condition, IL-6 secretion is normalized to total protein content in media. (*H*) Quantification of IL-6 in the BAL of saline-challenged $Myh11^{Cre}$ (n = 10), HDM-challenged $Myh11^{Cre}$ (n = 10), saline-challenged $STIM1^{smKO}$ (n = 9), and HDM-challenged $STIM1^{smKO}$ (n = 10) mice. $*P < 0.05$, $**P < 0.01$, $****P < 0.0001$ when compared to shScramble or saline-challenged $Myh11^{Cre}$, $\#P < 0.05$ when compared to HDM-challenged $Myh11^{Cre}$ (one-way ANOVA with Dunnett's test for multiple comparisons).

signaling downstream of STIM1. Similar results were observed when we studied a different batch of HASMCs originating from another donor (donor 2; *SI Appendix*, Fig. 5*J*). Furthermore, we validated these findings with the chronic asthmatic mouse model (Fig. 1*C*). We show that IL-6 secretion in the BAL of asthmatic mice challenged with HDM critically depends on ASM STIM1 (Fig. 4*H*). Using ELISA, HDM-challenged $Myh11^{Cre}$ mice had significantly more BAL IL-6 compared to saline-challenged $Myh11^{Cre}$ mice. Strikingly, BAL IL-6 was significantly reduced in the HDM-challenged $STIM1^{smKO}$ mice but was similar between the saline-challenged cohorts (Fig. 4*H*). As a control, we measured BAL Immunoglobulin E (IgE), which is predominantly secreted by plasma cells. Bal IgE was significantly increased in HDM-challenged mice compared to saline-challenged mice. Importantly, the BAL IgE levels of HDM-challenged $STIM1^{smKO}$ mice were statistically similar to those of HDM-challenged $Myh11^{Cre}$ mice. However, there was a trend for decreased BAL IgE in the HDM-challenged $STIM1^{smKO}$ mice, which may suggest a possible interaction of smooth muscle and plasma cells that is mediated by smooth muscle STIM1 (*SI Appendix*, Fig. 5*K*). These data strongly argue that the up-regulation of STIM1 specifically in ASM cells of asthmatic mice mediates IL-6 secretion through activation of NFAT4.

STIM1 Regulates ASM Proliferation and Migration through NFAT4. To establish that STIM1 regulates ASM proliferation and migration specifically through NFAT4 activation, we generated a constitutively active mutant of NFAT4 (CA-NFAT4) based on constructs previously reported (64, 65). Following the homology of a previously published constitutively active mutant of NFAT1 (66), we generated the CA-NFAT4 construct by introducing 25 alanine substitutions at serine phosphorylation sites in the SRR1, SP-1, SP-2, and SP-3 regions (*SI Appendix*, Fig. 6*A*). We added a carboxyl-terminal mCherry tag to this CA-NFAT4 construct and cloned it into a lentiviral vector to allow stable expression in HASMCs. Wild-type NFAT4mCherry and mCherry alone were also independently cloned into the same lentiviral vector. Unstimulated HASMCs expressed NFAT4mCherry primarily in the cytosol, and following thapsigargin stimulation, the construct translocated into the nucleus. The CA-NFAT4mCherry primarily localized to the nucleus in unstimulated HASMCs, suggesting constitutive activation of this construct (*SI Appendix*, Fig. 6*B*). We then expressed CA-NFAT4mCherry, NFAT4mCherry, and mCherry into stable shScramble, shSTIM1#1, and shSTIM1#5 HASMCs and measured proliferation and migration in complete culture media. Results from shSTIM1#1 and shSTIM1#5 were normalized to the respective shScramble. We found that CA-NFAT4 fully rescues proliferation and migration in shSTIM1#1 and shSTIM1#5 HASMCs (*SI Appendix*, Fig. 6 *C* and *D*). Interestingly, wild-type NFAT4 also rescued proliferation and migration in shSTIM1#1 and shSTIM1#5 HASMCs, although to a lesser extent than the constitutively active mutant. These results

suggest that wild-type NFAT4 overexpression in STIM1 KD cells likely leads to a significantly higher portion of NFAT4 migrating to the nucleus compared to cells expressing endogenous NFAT4 levels. These results show that STIM1 promotes ASM cell proliferation and migration through NFAT4.

Loss of STIM1 Quells ASM Cell Metabolism. An interesting finding that emerged from our transcriptional profiling and GSEA (Fig. 3 *A* and *B*) was that the "Diseases of Metabolism" pathway was significantly down-regulated in shSTIM1 HASMCs compared to shScramble HASMCs (Fig. 5*A* and *SI Appendix*, Fig. 7*A*). Recent studies suggest that ASM cells from asthmatic bronchi have enhanced respiration and mitochondrial mass and hypothesized that this augmented metabolism likely fuels AR (67, 68). Interestingly, recent evidence from T cells suggested that through activation of NFAT, SOCE is a major regulator of metabolic gene programs that support both oxidative phosphorylation and glycolysis (69). Thus, we evaluated mitochondrial respiration in HASMCs using the Seahorse mitochondrial stress test. Basal and maximal respiration were significantly reduced in shSTIM1#1 and shSTIM1#5 HASMCs compared to shScramble HASMCs (Fig. 5*B* and *SI Appendix*, Fig. 7 *B* and *C*). Nonmitochondrial respiration was unchanged (*SI Appendix*, Fig. 7*D*). Similar results were found with HASMCs obtained from another donor (donor 2; *SI Appendix*, Fig. 7*I*). Using qPCR, we found that mitochondrial DNA was significantly decreased in shSTIM1#1 and shSTIM1#5 KD HASMCs compared to shScramble HASMCs (Fig. 5*C*). Using transmission electron microscopy (TEM), we revealed that mitochondrial density was also considerably reduced in shSTIM1#1 and shSTIM1#5 KD HASMCs compared to shScramble HASMCs (Fig. 5 *D* and *E* and *SI Appendix*, Fig. 8*A*). Similarly, using flow cytometry, shSTIM1#1 and shSTIM1#5 KD HASMCs showed decreased Mitotracker staining compared to shScramble HASMCs (*SI Appendix*, Fig. 8*B*). Interestingly, TEM images showed that mitochondria were considerably longer in shSTIM1#1 and shSTIM1#5 KD HASMCs compared to mitochondria of shScramble HASMCs (Fig. 5 *D* and *F*). This includes a larger aspect ratio (Fig. 5*F*) and decreased circularity, roundness, and solidity in shSTIM1#1 and shSTIM1#5 KD HASMCs (*SI Appendix*, Fig. 8 *C–E*). In further support of this finding, the protein expression of mitofusin 2 (MFN2) and OPA1, which are two GTPases important for outer and inner mitochondrial membrane fusion, respectively (70), were significantly increased in shSTIM1#1 and shSTIM1#5 KD HASMCs compared to shScramble HASMCs (Fig. 5 *G–J*). However, we did not observe any changes in the expression of proteins of the electron transport chain (ATP5A, UQCRC2, MTCO1, SDHB, and NDUFB8) between shScramble, shSTIM1#1, and shSTIM1#5 HASMCs (*SI Appendix*, Fig. 8 *F* and *G*). Similarly, there was no change in protein expression of the mitochondrial biogenesis transcription regulators: peroxisome proliferator-activated receptor gamma coactivator 1-α (PGC1-α) and peroxisome proliferator-activated receptor-γ (PPAR-γ) between shScramble, shSTIM1#1, and shSTIM1#5 HASMCs (*SI Appendix*, Fig. 8 *H–K*). Proteins were quantified with the bicinchoninic acid (BCA) assay, equal amounts of total proteins were loaded for each condition, and GAPDH was used as a loading control. These results suggest that STIM1 regulates mitochondrial respiration, density, and fusion independently of the mitochondrial biogenesis pathways governed by PGC1-α and PPAR-γ.

Furthermore, using the Seahorse glycolytic stress test, we found that basal acidification, glycolysis, glycolytic capacity, and nonglycolytic acidification are decreased in shSTIM1#1- and shSTIM1#5-transfected HASMCs compared to shScramble HASMCs (Fig. 5*K* and *SI Appendix*, Fig. 7 *E–H*). Similar results were obtained with HASMCs originating from another donor (donor 2; *SI Appendix*, Fig. 7*J*). We also measured glucose consumption and lactate production in HASMCs using a YSI bioanalyzer. Compared to shScramble HASMCs, shSTIM1#1 and shSTIM1#5 HASMCs had significantly reduced glucose consumption and lactate production (Fig. 5 *L* and *M*). The protein expression of the major glucose uniporter in ASM cells, GLUT1 was also significantly decreased in shSTIM1#1 and shSTIM1#5 HASMCs compared to shScramble HASMCs (Fig. 5 *N* and *O*). Using liquid chromatography and mass spectrometry (Dataset S4), we also discovered that many amino acids are increased in shSTIM1#1 and shSTIM1#5 HASMCs compared to shScramble HASMCs (*SI Appendix*, Fig. 9 *A–C*), suggesting that preventing up-regulation of STIM1 leads ASM cells to accumulate amino acids that are otherwise used to support the proliferative smooth muscle phenotype.

STIM1^{smKO} HDM-Challenged Mice Show Decreased ASM Mitochondrial Density. Both the Myh11^{Cre} and STIM1$^{fl/fl}$ littermate mice were challenged with either saline or HDM in the chronic asthmatic mouse model (Fig. 1*C*). At day 49, fixed airways were embedded in TEM grids. ASM can be identified in the medial layers of airways (*SI Appendix*, Fig. 10*A*; red arrows). Consistent with previous findings (67, 68), mitochondrial density was significantly augmented in ASM of HDM-challenged Myh11^{Cre} mice compared to saline-challenged Myh11^{Cre} mice. Interestingly, and consistent with our in vitro results utilizing synthetic shSTIM1 KD HASMCs, HDM-challenged STIM1^{smKO} mice had considerably less mitochondrial density in their ASM than HDM-challenged Myh11^{Cre} mice. ASM cells from saline-challenged group mice had similar mitochondrial density (*SI Appendix*, Fig. 10 *A* and *B*). Consistent with the in vitro results utilizing synthetic shSTIM1 KD HASMCs, ASM cells from saline-challenged STIM1^{smKO} mice had elongated mitochondria with larger aspect ratio compared to ASM cells from saline-challenged Myh11^{Cre} mice, although this elongated mitochondrial phenotype was more drastic in cultured HASMCs (*SI Appendix*, Fig. 10*C*).

ASM STIM1 Promotes AHR and ASM Ca^{2+} Oscillations in Asthmatic Mice. Our mechanistic insights thus far show that inhibition of STIM1 expression in ASM cells leads to impaired NFAT4 activation, transcriptional reprogramming, and quelled metabolism. These data led us to hypothesize that HDM-challenged STIM1^{smKO} mice might have mitigated asthma manifestations. A cardinal feature of asthma is AHR, or the tendency of asthmatic airways to excessively contract in response to stimuli (71). Using the small animal ventilator, Flexivent, we measured AHR in living mice to the muscarinic agonist MeCh. HDM-challenged Myh11^{Cre} and STIM1$^{fl/fl}$ mice had enhanced AHR compared to saline-challenged Myh11^{Cre} mice (Fig. 6*A*). Astoundingly, HDM-challenged STIM1^{smKO} had significantly less AHR compared to HDM-challenged Myh11^{Cre} and STIM1$^{fl/fl}$ mice, while AHR was similar between the saline-challenged cohorts (Fig. 6*A*). These results strongly argue that ASM STIM1 is required for AHR in asthma.

To elucidate how ASM STIM1 regulates AHR, we considered the possibility that STIM1 in ASM cells may directly be modulating the Ca^{2+} signal generated by each dose of muscarinic agonist. Indeed, previous studies showed that agonist-induced rapid cytosolic Ca^{2+} oscillations are critical for ASM contraction (20, 72). SOCE, but not voltage-gated Ca^{2+} channels, has been shown as essential for maintaining Ca^{2+} oscillations in lung slices (73). To study agonist-induced Ca^{2+} oscillations in ASM from chronic asthmatic mice (Fig. 1*C*), we crossed STIM1^{smKO} and Myh11^{Cre} with GCaMP6$^{fl/fl}$ mice (74), and genotyping confirmed the insertion of the GCaMP6 cassette (*SI Appendix*, Fig. 11 *A* and *B*). This model allowed us to measure cytosolic Ca^{2+} oscillations specifically in ASM in live freshly isolated lung slices ex vivo. GCaMP6 fluorescence offered a large dynamic range as

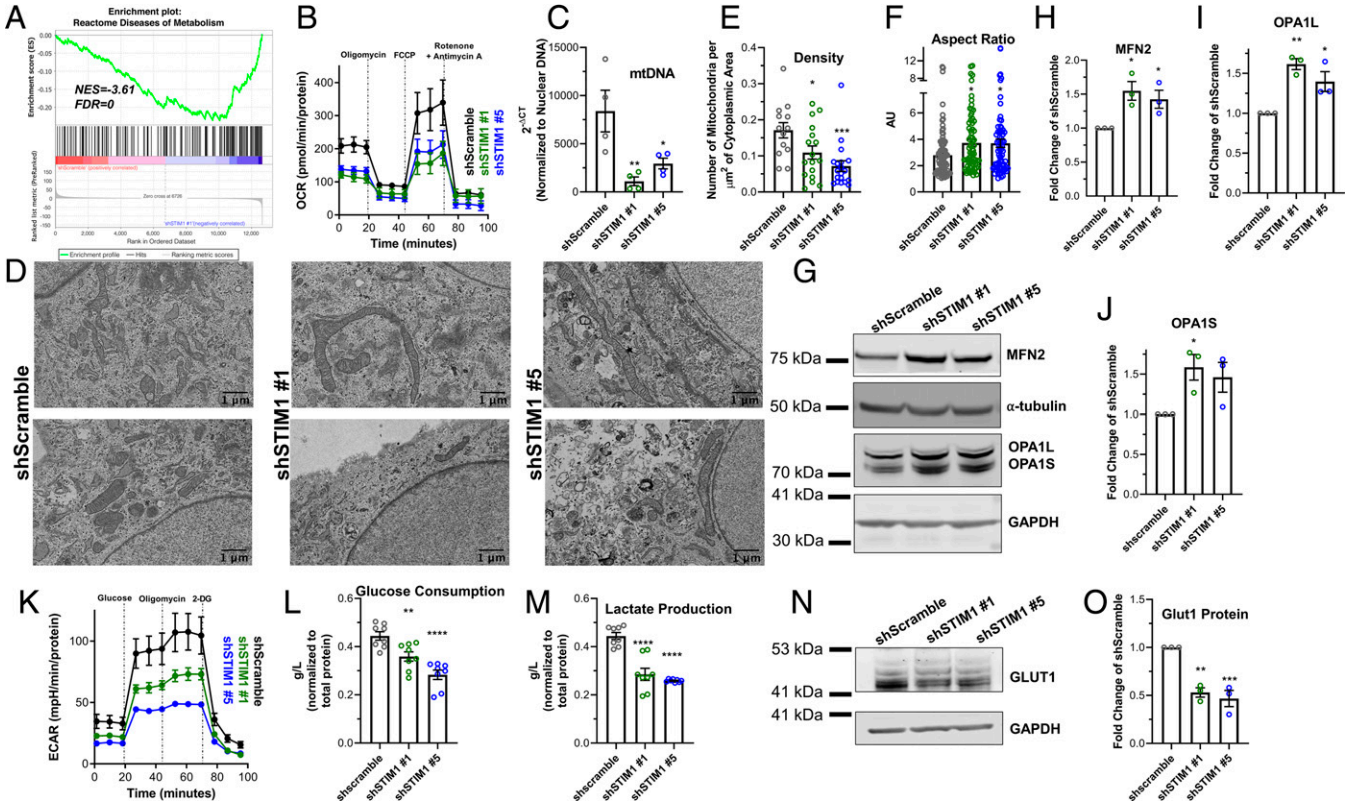

Fig. 5. STIM1 is crucial for metabolic activity of ASM cells. (*A*) GSEA enrichment plots using the reactome pathways gene set comparing shSTIM1#1 and shScramble HASMCs showing a negative correlation in the enrichment of diseases of metabolism. (*B*) Oxygen consumption rate (OCR) in shScramble (n = 7; black trace), shSTIM1#1 (n = 9; green trace), and shSTIM1#5 (n = 10; blue trace) HASMCs consecutively stimulated with 0.5 μM oligomycin, 2 μM Carbonyl cyanide-p-trifluoromethoxyphenylhydrazone (FCCP), and 0.5 μM rotenone/antimycin A. Measurements are normalized to total proteins in each sample. (*C*) Quantification of mitochondrial DNA (mtDNA) in shScramble (n = 4), shSTIM1#1 (n = 4), and shSTIM1#5 (n = 4) HASMCs using RT-qPCR. mtDNA cycle threshold (CT) values are normalized to CT values of genomic DNA products. (*D*) Two representative TEM images of shScramble, shSTIM1#1, and shSTIM1#5 HASMCs. (Scale bar: 1 μm.) (*E*) Quantification of the number of mitochondria per square micrometer of cytoplasmic area in micrographs from shScramble (n = 13), shSTIM1#1 (n = 17), and shSTIM1#5 (n = 19) HASMCs. (*F*) Quantification of the aspect ratio of mitochondria from shScramble (n = 99), shSTIM1#1 (n = 72), and shSTIM1#5 (n = 70) HASMCs. (*G*) Western blot showing MFN2, OPA1L, and OPA1S proteins in shScramble, shSTIM1#1, and shSTIM1#5 HASMCs. Quantification of MFN2 (*H*), OPA1L (*I*), and OPA1S (*J*) proteins from *G* in shScramble (n = 3), shSTIM1#1 (n = 3), and shSTIM1#5 (n = 3) HASMCs using densitometry normalized to α-tubulin and GAPDH. (*K*) Extracellular acidification rate (ECAR) in shScramble (n = 5; black trace), shSTIM1#1 (n = 7; green trace), and shSTIM1#5 (n = 6; blue trace) HASMCs consecutively stimulated with 10 mM glucose, 1 μM oligomycin, and 50 mM 2-deoxy-glucose (2-DG). Measurements are normalized to total proteins in each sample. Quantification of glucose consumption (*L*) and lactate production (*M*) in the media of shScramble (n = 8), shSTIM1#1 (n = 8), and shSTIM1#5 (n = 8) HASMCs using a bioanalyzer. (*N*) Representative Western blot showing GLUT1 protein in shScramble, shSTIM1#1, and shSTIM1#5 HASMCs. (*O*) Quantification of GLUT1 protein expression from *N* in shScramble (n = 3), shSTIM1#1 (n = 3), and shSTIM1#5 (n = 3) HASMCs using densitometry normalized to GAPDH. $^*P < 0.05$, $^{**}P < 0.01$, $^{***}P < 0.001$, $^{****}P < 0.0001$ (ANOVA with Dunnett's test for multiple comparisons).

determined by comparing unstimulated lung slices and maximally stimulated slices with 10 μM of the ionophore ionomycin (Fig. 6*B*). We then stimulated lung slices from saline-challenged and HDM-challenged Myh11^{Cre} and STIM1^{smKO} mice with the lowest concentration of MeCh (6.25 mg/mL) used in the AHR experiments. Six representative cells are shown in Fig. 6*C* for each of the four experimental conditions. We noted that ASM cells from the four different experimental conditions showed different proportions of four distinct patterns of Ca^{2+} signals in response to MeCh. These four patterns of Ca^{2+} signals are 1) cells that responded with a single transient that eventually receded to baseline (single spike); 2) cells that responded with repetitive Ca^{2+} oscillations; 3) cells that responded with a Ca^{2+} plateau for the duration of the recording; and 4) a subgroup of cells among the latter group (i.e., group 3) that responded with Ca^{2+} plateaus with regenerative Ca^{2+} oscillations on top of these plateaus (see *SI Appendix*, Fig. 12 for representative traces for each group of cells). We defined a Ca^{2+} oscillation as a spike that had an amplitude of at least 1.25-fold of the basal fluorescence value and returned to baseline. Plateaus were defined as sustained Ca^{2+} signals for at least 5 min after stimulation that receded to ≥25% of the initial peak. The proportion of cells with plateaus was calculated for each coverslip. For the cells without plateaus, the number of oscillations for that entire 14 min were reported.

Most ASM cells from control Myh11^{Cre} mice treated with saline responded with a Ca^{2+} plateau (55.4 ± 3.06%; Fig. 6*D*), with the remaining cells responding with a single spike (11.77 ± 1.8%) or with Ca^{2+} oscillations (32.82 ± 3.45%) as defined in Methods and in *SI Appendix*, Fig. 12. However, most ASM cells from STIM1^{smKO} mice treated with saline responded with Ca^{2+} oscillations (65.3 ± 4.65%; Fig. 6*D*) at the expense of Ca^{2+} plateaus (29.21 ± 5.0%) with 5.48 ± 1.63% of cells responding with a single spike, consistent with the requirement of STIM1 in supporting Ca^{2+} plateaus (29). Strikingly, in the HDM-challenged Myh11^{Cre} mice, the proportion of ASM cells that responded with Ca^{2+} oscillations increased significantly, (to 50.46 ± 5.56%) and among the cells that responded with plateaus (38.59 ± 5.95%), the majority (33.95 ± 5.7%) also displayed Ca^{2+} oscillations on top of these plateaus (Fig. 6*E*). ASM cells

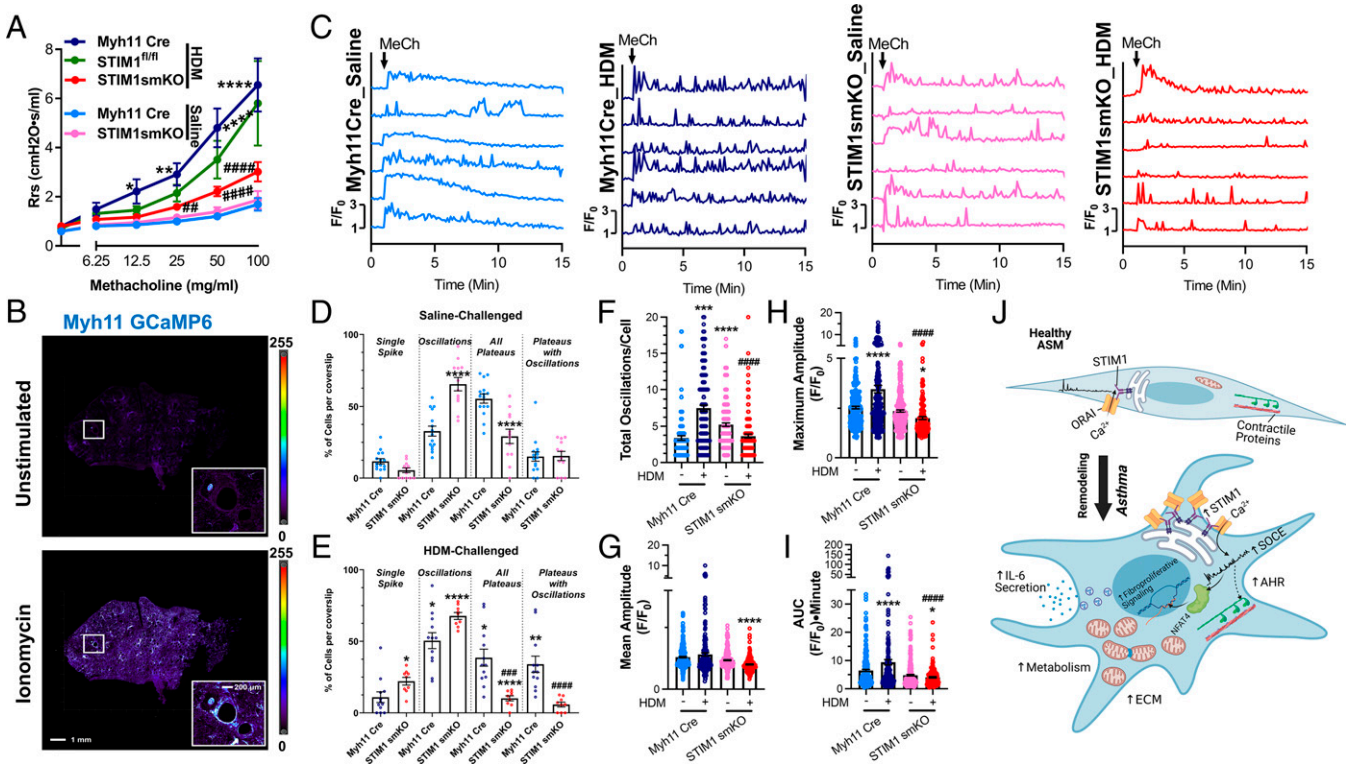

Fig. 6. ASM STIM1 is necessary for cytosolic Ca^{2+} oscillations and AHR. (*A*) Airway resistance (Rrs) in response to increasing concentrations of MeCh from saline-challenged Myh11^{Cre} (n = 12; light blue trace), HDM-challenged Myh11^{Cre} (n = 13; dark blue trace), HDM- challenged STIM1$^{fl/fl}$ mice (n = 5; green trace), saline-challenged STIM1^{smKO} (n = 12; pink trace), and HDM-challenged STIM1^{smKO} (n = 14; red trace) mice. (*B*) Representative confocal images of lung slices from Myh11^{Cre} mice expressing GCaMP6. The top image is unstimulated, and the bottom image is stimulated with 10 μM ionomycin in the presence of 2 mM Ca^{2+}. *Inset* displays an airway. (Scale bar: 1 mm and 200 μm for inset.) (*C*) Representative traces of Ca^{2+} oscillations in the ASM of lung slices from Myh11^{Cre} and STIM1^{smKO} mice expressing GCaMP6 and challenged with either saline or HDM. Lung slices were stimulated with 6.25 mg/mL MeCh in the presence of 2 mM Ca^{2+} at 1 min. Ca^{2+} oscillations are measured by the GCaMP6 fluorescence at each time point normalized to the GCaMP6 fluorescence at 0 min (F/F_0). (*D* and *E*) Quantification of the percentage of ASM cells responding with 1) a single Ca^{2+} spike, 2) regenerative Ca^{2+} oscillations returning to baseline, 3) all varieties of Ca^{2+} plateaus, and 4) a subset of Ca^{2+} plateaus from 3) 3 superimposed with Ca^{2+} oscillations in lung slices from (*D*) saline-challenged Myh11^{Cre} (n = 15, light blue circles) and saline-challenged STIM1^{smKO} (n = 12, pink circles) mice, and (*E*) HDM-challenged Myh11^{Cre} (n = 12, dark blue circles), and HDM-challenged STIM1^{smKO} (n = 9, red circles) mice. Representative movies of these four experimental conditions are SI movies S6 through S9, respectively. "n" represents the number of lung slices. Quantification in ASM cells of (*F*) total Ca^{2+} oscillations per 14 min, (*G*) mean amplitude, (*H*) maximal amplitude, (*I*) AUC of the Ca^{2+} signal for entire trace from saline-challenged Myh11^{Cre} (n = 108), HDM-challenged Myh11^{Cre} (n = 205), saline-challenged STIM1^{smKO} (n = 194), and HDM-challenged STIM1^{smKO} mice (n = 127). "n" represents number of ASM cells. *P < 0.05, **P < 0.01, ***P < 0.001, ****P < 0.0001 when compared to saline- challenged Myh11 Cre; ##P < 0.01, ###P < 0.001, ####P < 0.0001 when compared to HDM-challenged Myh11 Cre (one-way ANOVA with Dunnett's test for multiple comparisons). (*J*) Summary of the findings from this study (created with BioRender.com).

from HDM-challenged STIM1^{smKO} mice mostly responded with Ca^{2+} oscillations, with fewer cells displaying oscillations on top of plateaus (5.79 ± 1.65%; Fig. 6*E*). Importantly, although the vast majority of ASM cells from HDM-challenged STIM1^{smKO} mice responded with Ca^{2+} oscillations, they had significantly reduced Ca^{2+} oscillatory frequency (3.64 ± 0.27 oscillations/14 min compared to 7.5 ± 0.4 oscillations/14 min in the HDM-challenged Myh11^{Cre} group), with most cells showing a rundown of Ca^{2+} oscillations with time. Interestingly, the HDM-challenged STIM1^{smKO} ASM trended to have less Ca^{2+} oscillations than the saline-challenged STIM1^{smKO} ASM (Fig. 6 *C* and *F*). The reason for this difference requires further investigations, but it is possible that HDM causes changes in other proteins regulating the activities of either SOCE, IP_3 receptor–dependent Ca^{2+} release, or membrane potential.

When we considered the Ca^{2+} signals as a whole without distinction between the different patterns of Ca^{2+} signals, the mean of the amplitude, the maximum amplitude, and the area under the curve (AUC) of these Ca^{2+} signals were significantly larger in ASM cells from the HDM-challenged Myh11^{Cre} group compared to the other groups and were significantly blunted in ASM cells from the HDM-challenged STIM1^{smKO} mice (Fig. 6 *G*–*I*). These results suggest that during chronic asthma, most ASM cells respond with a high frequency of repetitive Ca^{2+} oscillations in response to agonists and that even cells responding with Ca^{2+} plateaus display oscillations on top of these plateaus. STIM1 is crucial for sustaining the high frequency and amplitude of these Ca^{2+} oscillations.

Discussion

It is clearly established that AR and, in particular, the increase of ASM mass are pathological hallmarks of asthma that contribute to disease severity (5, 8–10, 75–78). During ASM remodeling, ASM cells undergo a phenotypic switch from a quiescent to a synthetic phenotype (11, 12). The molecular mechanisms of this phenotypic switch remain largely unclear. Evidence points to an important association between ASM cell remodeling and the molecular reprogramming of surface receptors, ion channels, and Ca^{2+} signaling pathways. Specifically, STIM1, which is a critical component of SOCE in most cell types, is required for vascular smooth muscle remodeling in diseases such as chronic

hypertension and restenosis (26, 27, 41, 43). We previously showed that STIM1 protein is necessary for ASM cell proliferation and migration and that STIM1 expression is increased in ASM cells isolated from ovalbumin-challenged asthmatic mice (33). Others have shown that the pharmacological inhibitors of SOCE, 3,5-bis(trifluoromethyl) pyrazole and RP3128 mitigate airway inflammation and AHR in asthmatic rodent models (79–81). However, the specific role of ASM STIM1 in AR, AHR, and asthma has remained unknown. Although these SOCE inhibitors have questionable specificity, our work suggests that SOCE inhibition specifically in ASM through STIM1 deletion is sufficient to mitigate AR and AHR in asthma.

Here, we show that ASM STIM1 protein expression is increased in the chronic HDM-challenged asthmatic mice and that STIM1 is necessary for AR through activation of NFAT4. We show that HDM-challenged $STIM1^{smKO}$ mice have less airway fibrosis and reduced secretion of IL-6, a cytokine known to induce airway fibrosis (82). As the mechanisms of airway fibrosis are rather undefined (83), ASM cells have emerged as significant immunomodulatory cells capable of secreting cytokines and extracellular matrix (57). IL-6, which is also secreted by activated airway epithelial cells (62, 63), has been shown to stimulate smooth muscle cell proliferation and migration (60, 84). HDM has been demonstrated to induce SOCE-mediated production of IL-6 in airway epithelial cells (85). Hence, STIM1-mediated SOCE by HDM and agonists in airway cells and subsequent IL-6 secretion likely form a positive feedback loop that maintains AR. Our results show that IL-6 production requires activation of NFAT4, which agrees with previous studies (60, 86). STIM1 likely regulates the secretion of other profibrotic and inflammatory mediators by ASM. Indeed, our RNA sequencing showed that KD of STIM1 in HASMCs reduces the expression of transforming growth factor-β (TGF-β) and its receptor. Previous reports described a link between SOCE and fibrosis, presumably through SOCE-dependent up-regulation of TGF-β signaling (87, 88).

A striking finding from our transcriptional profiling experiments was that the asthma-associated gene ORMDL3 was down-regulated while muscle contractile pathways were positively enriched in our STIM1 KD HASMCs, suggesting that STIM1 KD in synthetic HASMCs induces cell differentiation back into the quiescent/contractile phenotype of healthy airways. Although further studies are required to understand the molecular mechanisms involved, STIM1-dependent signaling may serve as a molecular checkpoint in the dedifferentiation process of ASM remodeling. Previous studies showed that mitochondrial mass and metabolism are increased during AR in asthma (67, 68). A key discovery from our study is that STIM1 is a central driver of metabolic reprogramming that supports AR. Recent findings showed that SOCE is required for proliferation, secretion of cytokines, and clonal expansion of T cells through metabolic reprogramming and up-regulation of both oxidative phosphorylation and glycolytic genes (69). Interestingly, we found that STIM1 KD enhances MFN2 and OPA1 protein expression and ASM mitochondrial fusion. These data suggest that during AR, STIM1 is required for mitochondrial fission and enhanced mitochondrial function to bolster AR independently of mitochondrial biogenesis. Indeed, previous studies have shown that mitochondrial fission reflects a proliferative phenotype (89), while others reported that MFN2 expression is reduced in ASM of patients with asthma (90) and that cytokines induce mitochondrial fission in ASM (91). Future studies scrutinizing these proteins in isolated mitochondria would likely shed light on the specific pathways by which STIM1 controls mitochondrial density and dynamics.

Although AHR is a useful tool in the diagnosis and characterization of asthma (92), the molecular mechanisms of AHR are rather dubious (71). The contribution of AR to AHR is especially controversial. Some animal studies showed that overexpression of structural genes linked to asthma leads to AR and AHR in the absence of airway inflammation (93, 94), suggesting that AR contributes to AHR presumably because more and bigger ASM cells would support enhanced contractility (95). However, other studies have found no association between AR and AHR (96, 97). While our data showed that both AHR and AR are reduced in HDM-challenged $STIM1^{smKO}$ mice, STIM1 KD promotes the up-regulation of smooth muscle contractile genes. This suggests that AHR is likely mediated by receptor-dependent Ca^{2+} signaling pathways reminiscent of nonexcitable cells (e.g., SOCE) instead of voltage-dependent Ca^{2+} signaling (e.g., $Ca_V1.2$) commonly associated with muscle contractility. Clearly, additional studies are needed to determine any causal link between AR and AHR and the molecular pathways involved. Future studies with simultaneous contractility and Ca^{2+} imaging in isolated bronchial rings from the four different cohorts of mice studied herein would further elucidate the role of STIM1 and AR in airway contraction.

The enhanced frequency of Ca^{2+} oscillations has been recognized as an important determinant of AHR (73, 98, 99). In particular, it has been shown that the frequency of Ca^{2+} oscillations is directly related to the degree of sustained ASM contraction, which is important for AHR (99, 100). Frequent and repetitive Ca^{2+} oscillations are likely more adept at inducing sustained ASM contraction than monophasic Ca^{2+} spikes or plateaus that recede over time to near baseline. In addition, these signals are most likely driving the activation on long-term remodeling pathways such as ASM proliferation, migration, fibrosis, and IL-6 secretion. These Ca^{2+} oscillations are a product of agonist-induced ER Ca^{2+} release from the IP_3R (and, possibly, contributions from ryanodine receptors) and reuptake into the ER by SERCA (101). Our results demonstrate that ASM cells from HDM-challenged mice have increased Ca^{2+} oscillation frequency and amplitude compared to ASM cells from saline-challenged mice and present with a high proportion of ASM cells that respond with Ca^{2+} oscillations on top of sustained plateaus, which provides an explanation as to why asthmatic ASM exhibit AHR. Importantly, we show that ASM cells from HDM-challenged $STIM1^{smKO}$ mice have dramatically fewer Ca^{2+} oscillations than ASM cells from HDM-challenged $Myh11^{Cre}$ mice. Our results are consistent with previous pharmacological studies showing that SOCE, but not voltage-gated $Ca_V1.2$ Ca^{2+} channels, is important for maintaining Ca^{2+} oscillations in lung slices (73). Since STIM1 mediates significant molecular rewiring of ASM Ca^{2+} channels, receptors, and effectors during asthma, it is reasonable to propose that up-regulation of STIM1-mediated Ca^{2+} signals in asthmatic ASM cells mediates both short-term contractility that promotes AHR through receptor-evoked Ca^{2+} oscillations and long-term signaling that drives AR through NFAT4-dependent transcriptional and metabolic reprogramming. Future studies are needed to elucidate how these Ca^{2+} oscillations modulate smooth muscle contraction and how agonists and HDM itself, which has been shown to stimulate the protease-activated receptor expressed, drive AHR in asthma.

In summary, ASM STIM1 is up-regulated in asthma and is critical for both AR and AHR by mediating receptor-evoked Ca^{2+} signaling through SOCE, activation of Ca^{2+} oscillations in ASM, NFAT4, and downstream pro-remodeling transcriptional programs (Fig. 6*J*). Although, historically, Ca^{2+} chelators and L-type Ca^{2+} channel blockers showed disappointing efficacy in the treatment of asthma (102, 103), these treatments have likely failed to specifically target the unique spatiotemporal Ca^{2+} signals mediated by STIM1 that are necessary for AR and AHR. We propose that drugs that interfere with STIM1 function and block SOCE would likely be efficacious in alleviating AHR and AR in asthmatic patients. Since STIM1 and SOCE are also

critical for immune and epithelial cell function and these cell types are key components of airway inflammation in asthma (24), STIM1 and SOCE may represent the ideal target for asthma therapy.

Methods

HASMCs isolated from healthy and asthmatic donors were maintained in culture under standard conditions and used to perform biochemical assays, mitochondrial fuel flux assays, glucose and lactate measurements, and analysis of migration and proliferation. These cells were also transfected with shRNA against STIM1 and used in Ca^{2+} measurements using Fura2 and fluorescence microscopy. Ca^{2+} measurements on live lung slices from control and asthmatic mice were achieved through smooth muscle–specific expression of GCaMP6f in mice. Mitochondrial structure in HAMSCs and in lung slices from mice were studied using TEM. Lung function in anesthetized control and asthmatic mice was measured using the Flexivent system in which respiratory mechanics were evaluated in response to increasing doses of MeCh as described in detail in *SI Appendix*. All details of cell-culture conditions, complementary DNA construct cloning, stable expressions, Western blotting, RT-qPCR, Ca^{2+} imaging, proliferation and migration assays, flow cytometry, mitochondrial fuel flux assays, glucose and lactate measurements, transcriptome sequencing and analysis, TEM imaging, metabolomics, mouse models, AHR measurements, GCaMP6f measurements, IHC, IF (immunofluorescence), and BAL cell counts, and ELISA measurements are provided in *SI Appendix*. Details are also provided of sources and reference numbers for reagents, recombinant DNA, and oligonucleotides necessary for replication in *SI Appendix*.

Data Availability. All materials and experimental protocols, the sources and catalog numbers of reagents, sequences of oligonucleotides, sources of recombinant DNA, and genotypes and sources of animals necessary for replication of the study are included in *SI Appendix*. The source data has not been deposited in a publicly accessible database. All raw unprocessed data from the study are included in Dataset S1. Unprocessed gels and Western blots are included in Dataset S2. Raw RNA-sequencing data are included in Dataset S3, and raw metabolomics data are included in Dataset S4. All data are available upon request.

ACKNOWLEDGMENTS. We thank Drs. Yongsoo Kim and Steffy Manjila for using their vibratome and for help optimizing the conditions for GCaMP experiments, Dr. Han Chen from The Pennsylvania State University College of Medicine Electron Microscopy (EM) facility for assistance with TEM imaging, and Dr. Drew Jones and Mr. Leonard Ash from New York University Langone Health Metabolomics Core Resource Laboratory for assistance with metabolomics experiments. We are grateful to the Flow Cytometry and Informatic and Data Analysis Core facilities from The Pennsylvania State University College of Medicine. This work was supported by NIH/National Heart, Lung, and Blood Institute Grants R35-HL150778 (to M.T.), F30-HL147489-01A1 (to M.T.J.), TL1TR002016-04 (to M.T.J.), and P01-HL114471 (to R.A.P).

1. GBD 2016 Disease and Injury Incidence and Prevalence Collaborators, Global, regional, and national incidence, prevalence, and years lived with disability for 328 diseases and injuries for 195 countries, 1990-2016: A systematic analysis for the Global Burden of Disease Study 2016. *Lancet* **390**, 1211–1259 (2017).
2. T. Nurmagambetov, R. Kuwahara, P. Garbe, The economic burden of asthma in the United States, 2008-2013. *Ann. Am. Thorac. Soc.* **15**, 348–356 (2018).
3. K. F. Chung *et al.*, International ERS/ATS guidelines on definition, evaluation and treatment of severe asthma. *Eur. Respir. J.* **43**, 343–373 (2014).
4. P. Lange, J. Parner, J. Vestbo, P. Schnohr, G. Jensen, A 15-year follow-up study of ventilatory function in adults with asthma. *N. Engl. J. Med.* **339**, 1194–1200 (1998).
5. K. P. Hough *et al.*, Airway remodeling in asthma. *Front. Med. (Lausanne)* **7**, 191 (2020).
6. S. J. Wilson *et al.*, The relationship between eosinophilia and airway remodelling in mild asthma. *Clin. Exp. Allergy* **43**, 1342–1350 (2013).
7. A. Bourdin *et al.*, Specificity of basement membrane thickening in severe asthma. *J. Allergy Clin. Immunol.* **119**, 1367–1374 (2007).
8. S. Wadsworth, D. Sin, D. Dorscheid, Clinical update on the use of biomarkers of airway inflammation in the management of asthma. *J. Asthma Allergy* **4**, 77–86 (2011).
9. C. Pepe *et al.*, Differences in airway remodeling between subjects with severe and moderate asthma. *J. Allergy Clin. Immunol.* **116**, 544–549 (2005).
10. E. M. Rosethorne, S. J. Charlton, Airway remodeling disease: Primary human structural cells and phenotypic and pathway assays to identify targets with potential to prevent or reverse remodeling. *J. Exp. Pharmacol.* **10**, 75–85 (2018).
11. D. B. Wright *et al.*, Phenotype modulation of airway smooth muscle in asthma. *Pulm. Pharmacol. Ther.* **26**, 42–49 (2013).
12. S. Zuyderduyn, M. B. Sukkar, A. Fust, S. Dhaliwal, J. K. Burgess, Treating asthma means treating airway smooth muscle cells. *Eur. Respir. J.* **32**, 265–274 (2008).
13. D. C. Hill-Eubanks, M. E. Werner, T. J. Heppner, M. T. Nelson, Calcium signaling in smooth muscle. *Cold Spring Harb. Perspect. Biol.* **3**, a004549 (2011).
14. S. J. House, M. Potier, J. Bisaillon, H. A. Singer, M. Trebak, The non-excitable smooth muscle: Calcium signaling and phenotypic switching during vascular disease. *Pflugers Arch.* **456**, 769–785 (2008).
15. K. Mahn *et al.*, Diminished sarco/endoplasmic reticulum Ca2+ ATPase (SERCA) expression contributes to airway remodelling in bronchial asthma. *Proc. Natl. Acad. Sci. U.S.A.* **106**, 10775–10780 (2009).
16. M. C. Shepherd *et al.*, KCa3.1 Ca2+ activated K+ channels regulate human airway smooth muscle proliferation. *Am. J. Respir. Cell Mol. Biol.* **37**, 525–531 (2007).
17. V. A. Snetkov, S. J. Hirst, J. P. Ward, Ion channels in freshly isolated and cultured human bronchial smooth muscle cells. *Exp. Physiol.* **81**, 791–804 (1996).
18. Y. X. Wang, L. Wang, Y. M. Zheng, Canonical transient potential receptor-3 channels in normal and diseased airway smooth muscle cells. *Adv. Exp. Med. Biol.* **1131**, 471–487 (2020).
19. M. A. Thompson, Y. S. Prakash, C. M. Pabelick, Arachidonate-regulated Ca(2+) influx in human airway smooth muscle. *Am. J. Respir. Cell Mol. Biol.* **51**, 68–76 (2014).
20. J. A. Jude, M. E. Wylam, T. F. Walseth, M. S. Kannan, Calcium signaling in airway smooth muscle. *Proc. Am. Thorac. Soc.* **5**, 15–22 (2008).
21. C. Zhao *et al.*, Microdomain elements of airway smooth muscle in calcium regulation and cell proliferation. *J. Physiol. Pharmacol.*, 10.26402/jpp.2018.2.01 (2018).
22. M. Johnson, M. Trebak, ORAI channels in cellular remodeling of cardiorespiratory disease. *Cell Calcium* **79**, 1–10 (2019).
23. S. M. Emrich, R. E. Yoast, M. Trebak, Physiological functions of CRAC channels. *Annu. Rev. Physiol.*, 10.1146/annurev-physiol-052521-013426 (2021).
24. M. Prakriya, R. S. Lewis, Store-operated calcium channels. *Physiol. Rev.* **95**, 1383–1436 (2015).
25. M. Trebak, J. W. Putney Jr., ORAI calcium channels. *Physiology (Bethesda)* **32**, 332–342 (2017).
26. M. Potier *et al.*, Evidence for STIM1- and Orai1-dependent store-operated calcium influx through ICRAC in vascular smooth muscle cells: Role in proliferation and migration. *FASEB J.* **23**, 2425–2437 (2009).
27. W. Zhang *et al.*, Orai1-mediated I (CRAC) is essential for neointima formation after vascular injury. *Circ. Res.* **109**, 534–542 (2011).
28. R. E. Yoast *et al.*, The native ORAI channel trio underlies the diversity of Ca^{2+} signaling events. *Nat. Commun.* **11**, 2444 (2020).
29. S. M. Emrich *et al.*, Omnitemporal choreographies of all five STIM/Orai and IP_3Rs underlie the complexity of mammalian Ca^{2+} signaling. *Cell Rep.* **34**, 108760 (2021).
30. Y. Gwack, S. Feske, S. Srikanth, P. G. Hogan, A. Rao, Signalling to transcription: Store-operated Ca2+ entry and NFAT activation in lymphocytes. *Cell Calcium* **42**, 145–156 (2007).
31. O. Kudryavtseva, C. Aalkjaer, V. V. Matchkov, Vascular smooth muscle cell phenotype is defined by Ca2+-dependent transcription factors. *FEBS J.* **280**, 5488–5499 (2013).
32. S. E. Peel, B. Liu, I. P. Hall, ORAI and store-operated calcium influx in human airway smooth muscle cells. *Am. J. Respir. Cell Mol. Biol.* **38**, 744–749 (2008).
33. A. M. Spinelli *et al.*, Airway smooth muscle STIM1 and Orai1 are upregulated in asthmatic mice and mediate PDGF-activated SOCE, CRAC currents, proliferation, and migration. *Pflugers Arch.* **464**, 481–492 (2012).
34. N. Suganuma *et al.*, STIM1 regulates platelet-derived growth factor-induced migration and Ca2+ influx in human airway smooth muscle cells. *PLoS One* **7**, e45056 (2012).
35. A. Wirth *et al.*, G12-G13-LARG-mediated signaling in vascular smooth muscle is required for salt-induced hypertension. *Nat. Med.* **14**, 64–68 (2008).
36. M. Oh-Hora *et al.*, Dual functions for the endoplasmic reticulum calcium sensors STIM1 and STIM2 in T cell activation and tolerance. *Nat. Immunol.* **9**, 432–443 (2008).
37. L. N. Woo *et al.*, A 4-week model of house dust mite (HDM) induced allergic airways inflammation with airway remodeling. *Sci. Rep.* **8**, 6925 (2018).
38. Z. G. Chen *et al.*, Neutralization of TSLP inhibits airway remodeling in a murine model of allergic asthma induced by chronic exposure to house dust mite. *PLoS One* **8**, e51268 (2013).
39. S. Piñeiro-Hermida *et al.*, Attenuated airway hyperresponsiveness and mucus secretion in HDM-exposed Igf1r-deficient mice. *Allergy* **72**, 1317–1326 (2017).
40. J. M. Bisaillon *et al.*, Essential role for STIM1/Orai1-mediated calcium influx in PDGF-induced smooth muscle migration. *Am. J. Physiol. Cell Physiol.* **298**, C993–C1005 (2010).
41. M. T. Johnson *et al.*, L-type Ca^{2+} channel blockers promote vascular remodeling through activation of STIM proteins. *Proc. Natl. Acad. Sci. U.S.A.* **117**, 17369–17380 (2020).
42. F. C. Aubart *et al.*, RNA interference targeting STIM1 suppresses vascular smooth muscle cell proliferation and neointima formation in the rat. *Mol. Ther.* **17**, 455–462 (2009).
43. M. Kassan *et al.*, Essential role of smooth muscle STIM1 in hypertension and cardiovascular dysfunction. *Arterioscler. Thromb. Vasc. Biol.* **36**, 1900–1909 (2016).
44. R. A. Panettieri, R. K. Murray, L. R. DePalo, P. A. Yadvish, M. I. Kotlikoff, A human airway smooth muscle cell line that retains physiological responsiveness. *Am. J. Physiol.* **256**, C329–C335 (1989).
45. M. Trebak, STIM/Orai signalling complexes in vascular smooth muscle. *J. Physiol.* **590**, 4201–4208 (2012).

46. R. Berra-Romani, A. Mazzocco-Spezzia, M. V. Pulina, V. A. Golovina, Ca2+ handling is altered when arterial myocytes progress from a contractile to a proliferative phenotype in culture. *Am. J. Physiol. Cell Physiol.* **295**, C779–C790 (2008).
47. A. G. Porter, R. U. Jänicke, Emerging roles of caspase-3 in apoptosis. *Cell Death Differ.* **6**, 99–104 (1999).
48. A. K. Pham *et al.*, ORMDL3 expression in ASM regulates hypertrophy, hyperplasia via TPM1 and TPM4, and contractility. *JCI Insight* **6**, 136911 (2021).
49. G. R. Crabtree, E. N. Olson, NFAT signaling: Choreographing the social lives of cells. *Cell* **109** (suppl.), S67–S79 (2002).
50. X. Zhang *et al.*, A calcium/cAMP signaling loop at the ORAI1 mouth drives channel inactivation to shape NFAT induction. *Nat. Commun.* **10**, 1971 (2019).
51. A. S. Stevenson, M. F. Gomez, D. C. Hill-Eubanks, M. T. Nelson, NFAT4 movement in native smooth muscle. A role for differential Ca(2+) signaling. *J. Biol. Chem.* **276**, 15018–15024 (2001).
52. L. Zhao, M. N. Sullivan, M. Chase, A. L. Gonzales, S. Earley, Calcineurin/nuclear factor of activated T cells-coupled vanilliod transient receptor potential channel 4 ca2+ sparklets stimulate airway smooth muscle cell proliferation. *Am. J. Respir. Cell Mol. Biol.* **50**, 1064–1075 (2014).
53. S. Mancarella *et al.*, Targeted STIM deletion impairs calcium homeostasis, NFAT activation, and growth of smooth muscle. *FASEB J.* **27**, 893–906 (2013).
54. S. Feske, R. Draeger, H. H. Peter, K. Eichmann, A. Rao, The duration of nuclear residence of NFAT determines the pattern of cytokine expression in human SCID T cells. *J. Immunol.* **165**, 297–305 (2000).
55. S. Matsuda, S. Koyasu, Mechanisms of action of cyclosporine. *Immunopharmacology* **47**, 119–125 (2000).
56. M. Trebak, G. S. Bird, R. R. McKay, J. W. Putney Jr., Comparison of human TRPC3 channels in receptor-activated and store-operated modes. Differential sensitivity to channel blockers suggests fundamental differences in channel composition. *J. Biol. Chem.* **277**, 21617–21623 (2002).
57. G. Damera, O. Tliba, R. A. Panettieri Jr., Airway smooth muscle as an immunomodulatory cell. *Pulm. Pharmacol. Ther.* **22**, 353–359 (2009).
58. A. J. Ammit *et al.*, Tumor necrosis factor-alpha-induced secretion of RANTES and interleukin-6 from human airway smooth muscle cells: Modulation by glucocorticoids and beta-agonists. *Am. J. Respir. Cell Mol. Biol.* **26**, 465–474 (2002).
59. C. D. Huang, O. Tliba, R. A. Panettieri Jr., Y. Amrani, Bradykinin induces interleukin-6 production in human airway smooth muscle cells: Modulation by Th2 cytokines and dexamethasone. *Am. J. Respir. Cell Mol. Biol.* **28**, 330–338 (2003).
60. L. M. Nilsson *et al.*, Novel blocker of NFAT activation inhibits IL-6 production in human myometrial arteries and reduces vascular smooth muscle cell proliferation. *Am. J. Physiol. Cell Physiol.* **292**, C1167–C1178 (2007).
61. L. M. Nilsson-Berglund *et al.*, Nuclear factor of activated T cells regulates osteopontin expression in arterial smooth muscle in response to diabetes-induced hyperglycemia. *Arterioscler. Thromb. Vasc. Biol.* **30**, 218–224 (2010).
62. A. Jairaman, M. Yamashita, R. P. Schleimer, M. Prakriya, Store-operated Ca2+ release-activated Ca2+ channels regulate PAR2-activated Ca2+ signaling and cytokine production in airway epithelial cells. *J. Immunol.* **195**, 2122–2133 (2015).
63. T. S. Kountz *et al.*, Differential regulation of ATP- and UTP-evoked prostaglandin E_2 and IL-6 production from human airway epithelial cells. *J. Immunol.* **207**, 1275–1287 (2021).
64. K. Urso *et al.*, NFATc3 controls tumour growth by regulating proliferation and migration of human astroglioma cells. *Sci. Rep.* **9**, 9361 (2019).
65. T. Minami *et al.*, Vascular endothelial growth factor- and thrombin-induced termination factor, Down syndrome critical region-1, attenuates endothelial cell proliferation and angiogenesis. *J. Biol. Chem.* **279**, 50537–50554 (2004).
66. H. Okamura *et al.*, Concerted dephosphorylation of the transcription factor NFAT1 induces a conformational switch that regulates transcriptional activity. *Mol. Cell* **6**, 539–550 (2000).
67. P. O. Girodet *et al.*, Bronchial smooth muscle remodeling in nonsevere asthma. *Am. J. Respir. Crit. Care Med.* **193**, 627–633 (2016).
68. T. Trian *et al.*, Bronchial smooth muscle remodeling involves calcium-dependent enhanced mitochondrial biogenesis in asthma. *J. Exp. Med.* **204**, 3173–3181 (2007).
69. M. Vaeth *et al.*, Store-operated Ca^{2+} entry controls clonal expansion of T cells through metabolic reprogramming. *Immunity* **47**, 664–679.e6 (2017).
70. B. Westermann, Mitochondrial fusion and fission in cell life and death. *Nat. Rev. Mol. Cell Biol.* **11**, 872–884 (2010).
71. D. G. Chapman, C. G. Irvin, Mechanisms of airway hyper-responsiveness in asthma: The past, present and yet to come. *Clin. Exp. Allergy* **45**, 706–719 (2015).
72. M. J. Sanderson, P. Delmotte, Y. Bai, J. F. Perez-Zogbhi, Regulation of airway smooth muscle cell contractility by Ca2+ signaling and sensitivity. *Proc. Am. Thorac. Soc.* **5**, 23–31 (2008).
73. S. Boie, J. Chen, M. J. Sanderson, J. Sneyd, The relative contributions of store-operated and voltage-gated Ca^{2+} channels to the control of Ca^{2+} oscillations in airway smooth muscle. *J. Physiol.* **595**, 3129–3141 (2017).
74. L. Madisen *et al.*, Transgenic mice for intersectional targeting of neural sensors and effectors with high specificity and performance. *Neuron* **85**, 942–958 (2015).
75. T. R. Bai, Evidence for airway remodeling in chronic asthma. *Curr. Opin. Allergy Clin. Immunol.* **10**, 82–86 (2010).
76. J. K. Bentley, M. B. Hershenson, Airway smooth muscle growth in asthma: Proliferation, hypertrophy, and migration. *Proc. Am. Thorac. Soc.* **5**, 89–96 (2008).
77. M. Ebina, T. Takahashi, T. Chiba, M. Motomiya, Cellular hypertrophy and hyperplasia of airway smooth muscles underlying bronchial asthma. A 3-D morphometric study. *Am. Rev. Respir. Dis.* **148**, 720–726 (1993).
78. M. Ebina *et al.*, Hyperreactive site in the airway tree of asthmatic patients revealed by thickening of bronchial muscles. A morphometric study. *Am. Rev. Respir. Dis.* **141**, 1327–1332 (1990).
79. K. Ohga *et al.*, The suppressive effects of YM-58483/BTP-2, a store-operated Ca2+ entry blocker, on inflammatory mediator release in vitro and airway responses in vivo. *Pulm. Pharmacol. Ther.* **21**, 360–369 (2008).
80. M. Sutovska, M. Kocmalova, S. Franova, S. Vakkalanka, S. Viswanadha, Pharmacodynamic evaluation of RP3128, a novel and potent CRAC channel inhibitor in guinea pig models of allergic asthma. *Eur. J. Pharmacol.* **772**, 62–70 (2016).
81. T. Yoshino *et al.*, YM-58483, a selective CRAC channel inhibitor, prevents antigen-induced airway eosinophilia and late phase asthmatic responses via Th2 cytokine inhibition in animal models. *Eur. J. Pharmacol.* **560**, 225–233 (2007).
82. M. Rincon, C. G. Irvin, Role of IL-6 in asthma and other inflammatory pulmonary diseases. *Int. J. Biol. Sci.* **8**, 1281–1290 (2012).
83. S. G. Royce, V. Cheng, C. S. Samuel, M. L. Tang, The regulation of fibrosis in airway remodeling in asthma. *Mol. Cell. Endocrinol.* **351**, 167–175 (2012).
84. Z. Wang, W. H. Newman, Smooth muscle cell migration stimulated by interleukin 6 is associated with cytoskeletal reorganization. *J. Surg. Res.* **111**, 261–266 (2003).
85. A. Jairaman, C. H. Maguire, R. P. Schleimer, M. Prakriya, Allergens stimulate store-operated calcium entry and cytokine production in airway epithelial cells. *Sci. Rep.* **6**, 32311 (2016).
86. P. Tripathi *et al.*, Activation of NFAT signaling establishes a tumorigenic microenvironment through cell autonomous and non-cell autonomous mechanisms. *Oncogene* **33**, 1840–1849 (2014).
87. X. Mai *et al.*, Blockade of orai1 store-operated calcium entry protects against renal fibrosis. *J. Am. Soc. Nephrol.* **27**, 3063–3078 (2016).
88. B. Zhang *et al.*, Store-operated Ca^{2+} entry (SOCE) contributes to angiotensin II-induced cardiac fibrosis in cardiac fibroblasts. *J. Pharmacol. Sci.* **132**, 171–180 (2016).
89. M. Liesa, M. Palacín, A. Zorzano, Mitochondrial dynamics in mammalian health and disease. *Physiol. Rev.* **89**, 799–845 (2009).
90. B. Aravamudan *et al.*, Cigarette smoke-induced mitochondrial fragmentation and dysfunction in human airway smooth muscle. *Am. J. Physiol. Lung Cell. Mol. Physiol.* **306**, L840–L854 (2014).
91. P. Delmotte, G. C. Sieck, Interaction between endoplasmic/sarcoplasmic reticulum stress (ER/SR stress), mitochondrial signaling and Ca(2+) regulation in airway smooth muscle (ASM). *Can. J. Physiol. Pharmacol.* **93**, 97–110 (2015).
92. S. J. Fowler, O. J. Dempsey, E. J. Sims, B. J. Lipworth, Screening for bronchial hyperresponsiveness using methacholine and adenosine monophosphate. Relationship to asthma severity and beta(2)-receptor genotype. *Am. J. Respir. Crit. Care Med.* **162**, 1318–1322 (2000).
93. S. Das *et al.*, GSDMB induces an asthma phenotype characterized by increased airway responsiveness and remodeling without lung inflammation. *Proc. Natl. Acad. Sci. U.S.A.* **113**, 13132–13137 (2016).
94. M. Miller *et al.*, ORMDL3 transgenic mice have increased airway remodeling and airway responsiveness characteristic of asthma. *J. Immunol.* **192**, 3475–3487 (2014).
95. J. F. Perez-Zoghbi *et al.*, Ion channel regulation of intracellular calcium and airway smooth muscle function. *Pulm. Pharmacol. Ther.* **22**, 388–397 (2009).
96. J. A. Kermode *et al.*, The effect of airway remodelling on airway hyperresponsiveness in asthma. *Respir. Med.* **105**, 1798–1804 (2011).
97. B. E. McParland, P. T. Macklem, P. D. Pare, Airway wall remodeling: Friend or foe? *J. Appl. Physiol.* **95**, 426–434 (2003).
98. K. Parameswaran, L. J. Janssen, P. M. O'Byrne, Airway hyperresponsiveness and calcium handling by smooth muscle: A "deeper look". *Chest* **121**, 621–624 (2002).
99. J. F. Perez, M. J. Sanderson, The frequency of calcium oscillations induced by 5-HT, ACH, and KCl determine the contraction of smooth muscle cells of intrapulmonary bronchioles. *J. Gen. Physiol.* **125**, 535–553 (2005).
100. Y. Bai, M. J. Sanderson, Airway smooth muscle relaxation results from a reduction in the frequency of Ca2+ oscillations induced by a cAMP-mediated inhibition of the IP3 receptor. *Respir. Res.* **7**, 34 (2006).
101. M. J. Berridge, M. D. Bootman, H. L. Roderick, Calcium signalling: Dynamics, homeostasis and remodelling. *Nat. Rev. Mol. Cell Biol.* **4**, 517–529 (2003).
102. H. Downes, C. A. Hirshman, Calcium chelators increase airway responsiveness. *J. Appl. Physiol. (1985)* **59**, 92–95 (1985).
103. M. Ann Twiss, E. Harman, S. Chesrown, L. Hendeles, Efficacy of calcium channel blockers as maintenance therapy for asthma. *Br. J. Clin. Pharmacol.* **53**, 243–249 (2002).